Multi-stage micrite diagenesis in the late Jurassic of the Eastern Paris Basin: petrophysical and mechanical properties for engineering purposes

Benoit Vincent, Christophe Rigollet, Jean Cochard, Sara Khalil, Andrés Felipe Mejia-Duran, David Grégoire, Nicolas Beaudoin, Benjamin Brigaud, Thomas Blaise, Thierry Reuschle, et al.

Geological Society, London, Special Publications

Multi-stage micrite diagenesis in the late Jurassic of the Eastern Paris Basin: petrophysical and mechanical properties for engineering purposes

Benoit Vincent, Christophe Rigollet, Jean Cochard, Sara Khalil, Andrés Felipe Mejia-Duran, David Gregoire, Nicolas E. Beaudoin, Benjamin Brigaud, Thomas Blaise, Thierry Reuschle, Pierre Pellenard & Philippe Landrein

DOI: https://doi.org/10.1144/SP548-2023-139

To access the most recent version of this article, please click the DOI URL in the line above. When citing this article please include the above DOI.

Received 8 August 2023
Revised 17 December 2023
Accepted 15 January 2024

Multi-stage micrite diagenesis in the late Jurassic of the Eastern Paris Basin: petrophysical and mechanical properties for engineering purposes

Benoit Vincent[1], Christophe Rigollet[2], Jean Cochard[3], Sara Khalil[4], Andrés Felipe Mejia-Duran[7], David Gregoire[4,5,6], Nicolas E. Beaudoin[5], Benjamin Brigaud[6,7], Thomas Blaise[7], Thierry Reuschle[8], Pierre Pellenard[9] & Philippe Landrein[3]

[1]Cambridge Carbonates Ltd., Office 16, PMJ house, Highlands Road, Solihull, West Midlands, UK / 1 rue de varoux, 21120 Marey sur Tille, France

[2]CVA Group, 105 Av. Paul Doumer, 92500 Rueil-Malmaison, France

[3]Andra, Centre de Meuse/Haute-Marne, 55290 Bure, France

[4]Université de Pau et des Pays de l'Adour, LFCR, CNRS, E2S, 64600 Anglet, France

[5]Université de Pau et des Pays de l'Adour, LFCR, CNRS, E2S, TotalEnergies, 64000 Pau, France

[6]Institut Universitaire de France

[7]Université Paris-Saclay, CNRS, GEOPS, 91405 Orsay, France

[8]Université de Strasbourg, CNRS Institut Terre et Environnement de Strasbourg, UMR 7063, 5 rue René Descartes, Strasbourg F-67084, France

[9]Biogéosciences, UMR 6282 CNRS/uB/EPHE, Université de Bourgogne, 6 Bd Gabriel, 21000 Dijon, France

Corresponding author:

Benoit VINCENT

Cambridge Carbonates Ltd.

1 rue de Varoux, 21120 Marey sur Tille, France

Abstract

The "Calcaires du Barrois" Formation is a succession of dominantly micritic limestone of Kimmeridgian to Tithonian age, outcropping in the eastern part of the Paris Basin. This is an active karstic aquifer of main interest for the Andra (French National Agency for Radioactive Waste Management) who study the feasibility of a deep geological repository of radioactive waste in an Underground Research Laboratory (URL) located approximately 450m below the surface. Surface

installations of the CIGEO (Industrial Centre for Geological Disposal) project are planned to be located in the upstream recharge zone of the aquifer. It is of primary interest to characterise the "Calcaires du Barrois" Formation to provide guidelines for the planning and the sizing of these facilities, with the objective of minimising the impact on the aquifer system.

An integrated study was designed for this purpose linking petrography (thin section, and SEM, Scanning Electron Microscope), C & O stable isotope geochemistry, XRD (X-Ray Diffraction), petrophysics and geomechanics, and based on the analysis of three key cored wells penetrating the formation at different relative depths.

The "Calcaires du Barrois" underwent several stages of diagenesis that defined the current properties. Unconformities associated with the Jurassic-Cretaceous transition led to prolonged early subaerial exposures during which freshwater flowed efficiently through the upper half of the formation. Through mineralogical stabilisation, among other processes, microporosity was preserved in micrites in this interval consisting of clean limestone with thin marl layers. The lower half of the formation, more argillaceous, was not or only slightly affected by this early meteoric diagenesis and recrystallization and cementation of micrites occurred during burial diagenesis, involving chemical compaction. Later, during the return to the surface associated to the Cenozoic orogens, another phase of meteoric diagenesis affected the uppermost few metres below the outcropping portions of the formation, but without modifying significantly the previously acquired petrophysical properties. Consequently, an intra-formational boundary was progressively developed at around 75m (from the top reference). This boundary separates (1) a lower half of the "Calcaires du Barrois" with dense and tight micrites, showing high Young's Modulus values, and a moderate intensity of fractures, from (2) a upper half with microporous micrites showing low Young's Modulus values, and almost devoid of fractures. A transitional zone of about 30m-thick, with intermediate properties, sitting above this boundary and below the only thin metre-scale macroporous grainstone level of the formation, accommodated most of the deformation linked to the Cenozoic west-European orogens and is intensively fractured.

The current hydrogeological model considers a purely sedimentological boundary to delimit two sub-aquifers within the "Calcaires du Barrois" Formation, but will have to be reappraised since it is here demonstrated that the real boundary is located significantly higher in the formation and is inherited from a multi-stage diagenetic history. These findings will complement and influence planning for engineering of the CIGEO project.

Introduction

Micrite has been a subject of research for a long time, especially in relationship to oil and gas exploration. A first period of active investigation occurred in the 70's and 80's, with significant great advances mainly in the domains of morphology and mineralogy (e.g. Loreau, 1972; Moshier, 1989; Rezak and Lavoie, 1993). Following an interval of decreased interest in the 90's, a renewed research activity occurred especially focusing on the microporous reservoirs, and thus with a more developed petrophysical purpose (e.g. Lambert et al., 2006; Richard et al., 2007; Volery et al., 2009, 2010; Deville de Periere et al., 2011, 2017; Lucia and Loucks, 2013; Regnet et al., 2015). Diagenesis of micrite was almost always in the core of most of these studies (Hasiuk et al., 2016; Lucia, 2017; Hashim and Kaczmarek, 2019). Despite all these high quality works some key findings are still more admitted than really proven, such as the effect of clay content on the diagenetic evolution of micrites early suggested by Moshier (1989) and regularly mentioned and shown later on (e.g. Ehrenberg, 2004), but without being demonstrated. The implication of micrite diagenesis on the mechanical properties of fine crystalline limestone is even a very recent approach (e.g. Regnet et al., 2019).

The Andra (French National Agency for Radioactive Waste Management) studies the feasibility of a deep geological repository of radioactive waste in an Underground Research Laboratory (URL) located in the Eastern part of the Paris Basin (France). The laboratory is situated in a 150m-thick marl and mudstone strata at around 500m underground (Landrein et al., 2013), enclosed between two subsurface aquifers formed by Middle and Upper Jurassic limestones respectively (Linard et al., 2011). Surface installations of the CIGEO (Industrial Centre for Geological Disposal) project are planned to be located on and within the upstream zone of the active aquifer of the "Calcaires du Barrois" Formation of late Kimmeridgian to Tithonian age, mostly composed of fine crystalline limestone and a few marl interbeds. The hydrographic karstic network initiates in the study area and develops downstream towards the North and Northwest (Harmand et al., 2004; Jaillet, 2005). It is then of primary importance to characterise the "Calcaires du Barrois" Formation since the planning and sizing of the surface facilities, including the water protection and treatment units, will be done with the objective of minimising the impact on the aquifer system.

Three wells penetrated the "Calcaires du Barrois" Formation, forming a complete record of the entire succession. An integrated study of these wells was undertaken with petrographic investigations, carbon and oxygen (C & O) stable isotope analyses, X-Ray Diffraction (XRD) analyses, petrophysical measurements and geomechanical test, with the aim of characterising the formation and its properties. The objective is ultimately to understand the causes of the intra-formation

variability of these properties in order to better constrain the various aquifer characteristics in this upstream location.

Geological setting

The “Calcaires du Barrois” Formation crops out on the Eastern edge of the Paris Basin, forming an eastward convex U-shape outcrop band, like all the Jurassic outcrops in the area (Figure 1). The Andra defined a Zone of Interest for Detailed Surveys (ZIDS) within an area delineated by 3 main tectonic troughs, activated or re-activated during the Cenozoic tectonic movements (Pyrenean and Alpine orogens; e.g. André et al. 2006, 2010), and where the “Calcaires du Barrois” Formation is at the surface (Figure 1). The formation is an isopachous 130m-thick succession of limestones and a few marly interbeds of late Kimmeridgian to early Tithonian age, subdivided in 6 members (Figure 2). Laterally, the formation is extremely continuous over hundreds of kilometres from the North of Burgundy towards the Luxembourg, with the exception of the “Oolithe de Bure” Member which shows internal facies changes, and disappears towards the North (Collectif service DRD/MG, 2011; Brigaud et al., 2014).

The “Calcaires du Barrois” Formation records the deposition on a gently dipping homoclinal ramp during an overall 2nd order regression starting in the Kimmeridgian marls underlying the formation and ending, after the deposition of restricted Purbeckian facies, with a long-lasting interval of subaerial exposure and karstification related to the Late Cimmerian Unconformity (LCU; Jacquin et al., 1998; Brigaud et al., 2018). The internal members within the formation, initially defined by Mégnien and Mégien (1980), most likely illustrate the influence of 3rd order variations within the 2nd order regression. They were described and interpreted in detail by Pellenard et al. (2011), whose finding are discussed hereafter.

The lower 3 members, namely the “Calcaires sublithographiques”, the “Pierre châline” and the "Calcaires de Dommartin”, with respective thicknesses of 20-30m, 10m and 60.5m, mostly comprise argillaceous bioturbated bioclastic wackestone with bivalve shell debris, echinoderm debris, brachiopod shells, agglutinated foraminifers with also a few small benthic foraminifers, serpulids (encrusting and not), and with some silt-sized quartz grains. Note that the “Calcaires de Dommartin” Member is divided in 3 sub-members, lower, mid and upper. The “Pierre châline” and the middle part of the “Calcaires de Dommartin” contain marl interbeds with centimetre to decimetre-scale bioclastic layers of oyster shells and echinoids, forming local flow barriers in the “Calcaire du Barrois” hydrological system. Quartz grains disappear and clay content significantly decreases in the upper

"Calcaires de Dommartin", the facies becoming cleaner. The facies of the lower part of the formation are characteristics of deposition in middle ramp settings (sensu Burchette and Wright, 1992).

The 2m-thick "Oolithe de Bure" member corresponds to a cross-bedded oobioclastic grainstone, with variable relative amounts of ooids and bioclasts in the study area and capped by a hardground. These facies characterize an inner ramp high energy setting (sensu Burchette and Wright, 1992). The two upper members, with respective thicknesses of 20-30m and 2-3m, are the "Calcaires cariés et tachetés" and the "Calcaires tubuleux". They consist of relatively clean wackestone to packstone with bivalve shell debris, gastropod debris, green algae, and small benthic foraminifera including miliolids, with locally some peloidal grainstone lenses. These limestones are intensively bioturbated, showing a dense network of *Thalassinoides* traces, and the top of the upper member is a hardground. These limestones were interpreted by Pellenard et al. (2011) as deposited in a middle ramp setting, similarly to the facies of the lower part of the formation. However, the faunal assemblages are significantly different in the two intervals, the upper one being more characteristic of inner ramp low energy settings (sensu Burchette and Wright, 1992). This re-interpretation is more consistent with the regional and supra-regional stratigraphic scheme of a deposition during a 2nd order regression (Jacquin et al., 1998).

The "Calcaires du Barrois" and overlaying Purbeckian facies were covered by 300±200m of Cretaceous sediments including early Cretaceous, mostly clastic deposits, and late Cretaceous chalk (Blaise et al., 2014). The Cenozoic orogens removed this sedimentary cover progressively, bringing back the formation to the surface, where it was affected by karstic alteration (Harmand et al., 2004; Moreau et al., 2023). This resulted in a complex interplay between the late Jurassic to earliest Cretaceous paleokarst system, and the recent karst (e.g. Jaillet, 2005).

Material and methods

Three wells were drilled within the ZIDS in the "Calcaires du Barrois" Formation, EST-1201, EST-1203, and EST-1218 (Figure 1). Fully cored, the wells are not equivalent because they penetrated the formation at different stratigraphic levels due to their respective geographical location; they are perfectly complementary stratigraphically and form an almost continuous record of the formation. EST-1218 cuts through the lower members whereas EST-1203 is in an intermediate position, with no direct superposition between the two wells (Figure 3). EST-1201 concerns the upper members and shows an interval of superposition of 17m with EST-1203 in the upper part of the "Calcaires de Dommartin" Member. Because of the effects of the LCU unconformity and the associated erosion and karstification, the top of the "Calcaires du Barrois" Formation, despite having been deposited

everywhere, is heterogeneously preserved. In EST-1201, at 15m depth, Valanginian clastics are sitting directly on the "Calcaires cariés et tachetés" which are incomplete.

A total of 135 samples were taken from the 3 cores for a set of analyses. Thin sections impregnated with blue dyed epoxy and fully stained for carbonates (Lindholm and Finkelman, 1972) were prepared for 24 samples. Cathodoluminescence (CL) observations were realised at GEOPS (Paris-Saclay University) on the thin section with grainstone textures, i.e. the samples from the "Oolithe de Bure" Member. Investigations were performed using a Cathodyne cold-cathode cathodoluminescence from NewTec operating at 14kV and 150 to 250µA, coupled to an Olympus microscope and a Qicam Fast 1394 digital camera.

The large dominance of mud-supported textures, except in the "Oolithe de Bure" Member, necessitated the use of Scanning Electron Microscope (SEM), in order to investigate the micrite morphology. Six samples were chosen for SEM observations, for which both freshly fractured and polished impregnated small cubes of rocks (0.5x0.5x1cm) were prepared. They were observed on an IT100 JEOL SEM with accelerative voltages of 3Kv to 7kV. Image analysis and crystal size measurement were performed by the JMicrovision © software.

Fracture and stylolite intensity were semi-quantified visually on cores, using three classes, low, moderate, and high. Semi-quantification was realised by steps of 10cm in the well-preserved intervals and 30cm in more damaged zones of the cores.

Bulk-rock XRD analyses were performed in the laboratory of the University of Burgundy. A total of 73 powders were analysed with a Bruker D4 Endeavor diffractometer with the following characteristics: a type Kα-1Cu cathode, a Ni filter, a fast LynxEye detector, operating tension and intensity of respectively 40kV and 25mA, 15 rounds/min, a step of 0.0399°, a screening window of 3° to 60° 2Θ, and a scan duration of 11 mins and 40 secs. Mineral phases were identified with the use of Mac Diff (4.2.5) software.

C & O stable isotope ratio ($\delta^{13}C$ and $\delta^{18}O$) of calcite were acquired using isotope ratio mass spectrometer (IRMS). Analyses were performed from 70 bulk rock powders sampled with a1 mm-diameter dentist microdrill. Sampling focused on homogeneous micrites devoid of bioclasts or fractures, with the noticeable exception of the few grainstone textures in the "Oolithe de Bure". Carbonate powders were analysed using a dual-inlet Isoprime 100 spectrometer (Elementar) coupled to a multiCarb system at the "Laboratoire des Sciences du Climat et de l'Environnement" (Paris-Saclay University). Data were standardized to Pee Dee Belemnite (PDB) based on repeated measurements of international reference materials NBS19 and NBS18, with respective values of -

2.20 ‰ and -23.01 ‰ in PDB for $\delta^{18}O$ and 1.95 ‰ and -5.01 ‰ in PDB for $\delta^{13}C$. The uncertainties reported are based on the external reproducibility of an in-laboratory carbonate standard (MARGO) with 1SD of 0.05 ‰ for $\delta^{18}O$ and 0.03 ‰ for $\delta^{13}C$. All results are presented in per mil (‰) deviation from the PDB standard (‰ PDB). The bulk rock dataset was completed by a set of analyses performed by Pellenard et al. (2011) on Low Magnesian Calcite (LMC) shells sampled in the 3 cored wells. All results are provided in Table 1.

Permeability (K) and porosity (ϕ_t) were measured on respectively 51 and 37 samples, mostly concentrated in the lower part of the "Calcaires du Barrois" Formation. Permeability was acquired in a nitrogen Hassler cell permeameter and corrected for the Klinkenberg effect. Porosity was measured by Mercury Injection Porosimetry (MIP; e.g. Zinszner and Pellerin, 2007) using a Micrometrics Auto Pore IV 9500 apparatus in the Laboratory of the University of Pau. This dataset was completed by 81 porosity and permeability data from Pellenard et al. (2011) covering the entire formation. The latter set implied a different technique for total porosity measurement, by weighting dried versus fully vacuum water-saturated samples. But the 2 datasets display very similar values for the same stratigraphic intervals (Figure 4). Also, Pellenard et al. (2011) measured the 48h-porosity (ϕ_{48h}) or free porosity as defined by Mertz (1991) and following the AFNOR B.10.513 standard, on the same set of samples. This corresponds to the pore volume accessible by simple imbibition of water under atmospheric pressure in the presence of air (2 cycles of 24h). Most of the time the ϕ_{48h} is lower than ϕ_t because air bubbles are trapped within the largest pores. A saturation coefficient S_{48} is defined, allowing to appreciate relatively quickly some aspects of the pore network:

$$S48 = \frac{\phi 48h}{\phi t}$$

Mechanical properties were determined all through the formation, by an integrated method additioning Ultrasonic Pulse Velocity (UPV) tests on samples, mechanical tests on samples, and Schmidt hammer rebound measurements on cores. Six sets of samples, two per well, each covering a 1.5m-thick interval of cores, were chosen from the most homogeneous zones. Within each of these intervals, 4 plugs were extracted to estimate the Dynamic Young's Modulus (E_d), by the measurement of P and S wave velocities using a Prosceq Pundit 200 UPV with 2 Olympus normal incidence shear wave 0.25MHz transducers. Twenty-four travel times T_p and T_s, respectively associated with P-waves and S-waves, were measured, and velocities were calculated as:

$$Vp = \frac{L}{Tp}$$

$$Vs = \frac{L}{Ts}$$

where L is the length of the plug.

The bulk and shear moduli, K and G respectively, were calculated by:

$$Vp = \sqrt{\frac{K + \frac{4}{3}G}{\rho}}$$

$$Vs = \sqrt{\frac{G}{\rho}}$$

where ρ is the sample density.

Finally, E_d was calculated with:

$$\mathrm{Ed} = 2\mathrm{G}(1 + \nu) \; or \; \mathrm{Ed} = 3\mathrm{K}(1 - 2\nu)$$

with ν being the Poisson's ratio:

$$\nu = \frac{3K - 2G}{2(3K + G)}$$

Mechanical tests were performed on 4 of the plugs selected for the UPV tests to estimate the Young's Modulus E. A Zwick HB250 testing appartus was used and the sample (with a minimum height of 2 times the diameter) was attached to 3 sensors situated at 120°. Each sensor estimated the displacement that the plug underwent on 3 sides after being exposed to a load of maximum 4KN and minimum 1KN. The plugs were centred under the jack hammer and a minimum of 3 cycles were performed. A linear function was established with the 4 test plugs between the UPV-derived E_d and the measured E, with a R^2 of 0.91. Using this function, values of E were calculated for the remaining 20 plugs.

A total of 133 Schmidt hammer rebound measurements were also performed through the cores in the most continuous way as possible depending on the quality of the cores. A minimum of ten rebounds (unitless) were collected on each target points, and mean values per target point were calculated. Any occurrence of a break or slighter damage at the core surface during the cycle of acquisition at one site led to the deletion of the point. Rebounds were collected close to the location of 9 of the 24 reference plugs. A linear function was established between these 9 rebound values (R) and the calculated E values of the corresponding 9 plugs, with a R^2 of 0.94 (E=2.0889 x R -47.936,

with E in GPa). This resulted in a final relatively continuous set of calculated 126 values of Young's Modulus E through the 3 wells, 86 in EST-1218, 15 in EST-1203, and 25 in 1201.

In order to confirm the reliability of the Schmidt hammer-derived Young's Modulus E values, Triaxial tests were also performed on a set of 6 samples, 3 from mudstone to wackestone of "Calcaires de Dommartin inférieurs", and 3 from the grainstone of the "Oolithe de Bure" (Table 2). Each set of 3 samples were taken in an interval of less than 1m thick. Samples were cut with a rock saw to make flat surfaces and then cored parallel to bedding/lamination using a diamond tipped core bit and a glass core bit of 19.8mm diameter. Care was taken to avoid visible fractures or veins. Core plugs were trimmed using a diamond tipped saw. Cores were cut as long as possible, however some cores were not long enough to use in strength tests, where the ratio of diameter to length needs to be 1:2 or 1:2.5 (Jaeger and Cook, 1969). All cores used in strength tests were precision squared using a diamond tipped steel grinding wheel so that their ends were flat and parallel. Prior to testing all core plugs were dried in an oven at 80°C. Each sample was deformed in a triaxial mechanical cell at the University of Strasbourg (France), with a pore pressure of 10 MPa, increasing normal stress and at different confining pressures for each sample of a given set that allow building the Mohr Coulomb criterion. For the "Oolithe de Bure" samples, deformation was done at confining pressures of 15, 17.5 and 20 MPa, calculation of the E value based on the slope of the elastic load-up returned an average value of 3.5GPa, which is in line with the mean value of the 3 nearest Schmidt hammer-derived E values of 13.5GPa. It also allowed to calculate the cohesivity of the material (0.2 MPa) and the internal frictional angle (7.5°). For the "Calcaires de Dommartin inférieurs", the 3 samples were deformed at confining pressures of 20, 30 and 40 MPa, returning mean value of 36.4GPa, also in line with the 3 closest Schmidt hammer-derived E values of 53.7GPa. It also allowed to calculate the cohesivity of the material (22 MPa) and the internal frictional angle (32°). Despite the rock being very heterogeneous at the cm-scale, mechanical tests and Schmidt hammer results show consistency at the first order, the orders of magnitudes and trends being compatible between methods and members. This confirms the reliability of using the rebound value as a proxy for the Young's Modulus as developed in this project.

Results

All the analytical results are presented in a synthetic Figure 4, integrating the data acquired in this work and the complementary datasets. Results are described hereafter by sets of analysis.

Macroscopic and microscopic Facies characteristics

There are no limestone-marl alternations (LMA; e.g. Westphal et al., 2008) in the "Calcaires du Barrois" Formation, but some do exist within the underlying Kimmeridgian "Marnes à exogyres" Formation. The "Pierre châline" Member displays some bioclastic argillaceous beds non-rhythmically interbedded in finer carbonate-richer beds, which is almost the reverse of the classical pattern observed in LMAs (Westphal et al., 2008). Consequently, it is likely that the micritic carbonates under study are not mostly derived from early diagenetic processes as described by Munnecke et al. (2023), but are of primary origin and were diagenetically altered.

The base of the "Calcaires du Barrois" Formation is largely dominated by wackestone textures, with rare cm-scale packstone layers, and were calcitic elements such as echinoderms, bryozoans, brachiopod, and serpulids, are dominant, but with also a few bivalves are rarer gastropod debris (Figure 5C). In this lower part of the formation, the dominant pore-type is microporosity within micrite of the matrix, micritisation of grains being limited. Microporosity is visible through a faint blue stain due to limited epoxy impregnation, and is limited to the vicinity of open microfractures, or stylolites (Figure 5E).

The facies evolve towards the top, although textures are remaining largely dominated by wackestone, and subsidiary packstone. Calcitic elements are decreasing in abundance but are still present, notably echinoderms, and the abundance of aragonite bioclasts such as gastropod and green algae debris increases upwards. Microporosity within micrite of matrix and grains is still the dominant pore-type, but macro- and micro-moulds are present in the upper part of the formation (Figure 5A, B; Figure 7B). Microporosity is more homogeneously distributed, and less restricted to the vicinity of microfractures, which are less abundant.

The "Oolithe de Bure" Member is a break in this lime mud-dominated succession, where the exclusive facies is bioclastic and peloidal grainstone, with clear cross-bedding on cores. The grainstones are first partially cemented by eogenetic (1) isopachous rims of dirty/inclusion-rich circumgranular calcite (Figure 6A, C), visible around grains but not within moulds of aragonitic bioclasts; and (2) contemporaneous inclusion-rich syntaxial overgrowths around echinoderm debris (Figure 6A, B). The isopachous rims display a dull dark luminescence under CL (Figure 6D), indicating, together with the previous characteristics a probable marine origin (e.g. Aissaoui, 1988). These eogenetic cements are post-dated by a clear equant calcite cement showing a sector zoning under CL (Figure 6D), most probably precipitated during burial. The latter cement occurs within interparticle pores, where it also forms a second phase of syntaxial overgrowth, and moulds. These successive cements did not plug entirely the porosity and a significant open interparticle and mouldic porosity is preserved in that Member (Figure 6A, C). Noteworthy is the presence of possible

fitted fabric grainstone in the interval, probably indicating subaerial exposures (Figure 6B; Smith, 2023).

Pellenard et al. (2011) mention a vertical evolution of micrite textures through the formation. Indeed, the lower part is characterized by dense micrites with coalescing anhedral fitted crystals (Figure 7C, D), corresponding to the Type III textures sensu Kaczmarek et al. (2015), with a mean crystal size around 5-6µm. The upper part mostly shows some porous micrites with subhedral crystals (Figure 7A, B), corresponding to the Types I-II sensu Kaczmarek et al. (2015), and with a mean crystal size around 2-3µm. The change occurs through the stratigraphic intervals covered by EST-1203 and is illustrated by two samples taken at the base and the top of this well. The two micrite textures are not extremely dissimilar visually on SEM images, with respectively a Type II to III texture for the lower sample (Figure 8 left side), and a Type I to II texture for the upper sample (Figure 8 right side). The mode of crystal size is similar in both samples (Figure 8), but the distribution of the sizes in the lower sample shows a shoulder towards larger crystals (Figure 8 right side). As a result, the samples display significantly distinct modes of pore-throat sizes, with respectively 0.07µm and 0.4µm for the lower and upper samples.

Stylolites are abundant in the lower half of the formation where they are thin and low amplitude, and often coalesce to form solution seams (Figure 9). They are almost absent in the upper half, with however two zones of occurrence between 55m and 62m, and 23m to 30m (Figure 14). In these 2 intervals, they are still thin but slightly higher amplitude (Figure 9). Fractures, mostly consisting of thin, discontinuous, and short (centimetre to decimetre-scale) features, are present all through the stratigraphic interval. They are sometimes calcite-cemented, mostly partially, and sometimes open (Figure 9). They are significantly present in the lower half of the formation, very abundant between 75m and 45m, and much rarer in the uppermost part (Figure 14).

XRD data

XRD data show an increasing-upward content of the carbonate fraction. This is consistent with the cleaning-up trend of the Gamma-Ray (GR), illustrated by the upward decrease of spikes within an overall low signal (Figure 4). The lowermost Member of the “Calcaires sublithographiques” is already carbonate-rich but still almost marly at its base, above the Kimmeridgian “Marnes à exogyres” Formation. Every GR kicks in the overlying members correspond to slight lows of carbonate content. This is particularly visible in the “Pierre châline”, the upper “Calcaires de Dommartin inférieurs” and in the “Calcaires de Dommartin supérieurs” members. In EST-1201, the “Calcaires cariés et tachetés” Member reveals a high carbonate content, but also shows some small GR peaks, which probably

record the clayey infill of recent small karst features, some being possibly developed from the dense network of burrows present in this upper part.

Stable isotopes

The bulk $\delta^{18}O$ values show limited variations through the studied stratigraphic interval, ranging between -1‰ and -3‰ mostly, with a few exceptions mainly encountered in and above the "Oolithe de Bure" Member where the range is larger (Figure 4). On the contrary, the $\delta^{18}O$ of shells are increasing from base to top, becoming even positive slightly below the "Oolithe de Bure" Member. This rise was interpreted by Pellenard et al. (2011) as illustrating a most probable cooling in the late Tithonian. Bulk data are mostly more negative than the stratigraphic equivalent shell data, but nevertheless increase around the later Member, partially keeping a trace of the initial seawater record. The bulk $\delta^{13}C$ values show a distinct evolution, with a slight but continuous decrease through the "Calcaires du Barrois"; this decrease is not visible in the values of the shells, remaining between 2‰ and 3‰ all along (Figure 4).

The upper part of the formation is characterised by an erratic bulk $\delta^{18}O$ signal, with in particular a very negative value for a sample of the "Oolithe de Bure" Member (Figure 4). Sampling did not allow to segregate the various components of the grainstones, and it is probable that the negative $\delta^{18}O$ value illustrates the influence of the burial cements. Such cements most likely precipitated from fluids at moderately elevated temperatures (lower than 50°C) considering the limited burial (Blaise et al., 2014), similarly to what happened in the underlying Oxfordian and Bathonian limestone (Vincent et al., 2007; Brigaud et al., 2009). However, the influence of subaerial exposures, identified through some possible fitted grainstone fabrics, cannot be ruled out, the $\delta^{13}C$ of the sample also being slightly lower than the values of the surrounding samples. Two $\delta^{13}C$ bulk values are very low, one being even negative, and out of the trend, both located within the "Calcaires cariés" Member (Figure 4). The $\delta^{18}O$ of these samples are also somewhat more negative than the surrounding samples. These values illustrate the likely existence of subaerial exposure surfaces close to the top of the member. The cores in this interval of the well EST-1201 are intensively bioturbated, but some of the burrows may have been enlarged by dissolution. A more thorough examination and analysis of this interval may however be necessary to confirm this point.

A classical $\delta^{18}O$ vs. $\delta^{13}C$ cross-plot also reveals the trends described above (Figure 10). A net increase of shell $\delta^{18}O$ values is observed from EST-1208 to EST-1201, thus from the base to the top of the formation, whereas $\delta^{13}C$ remains stable. Bulk $\delta^{18}O$ and $\delta^{13}C$ values are respectively slightly rising and more significantly decreasing at the same time. In order to avoid being influenced by extreme values

or outliers in the curves or the cross-plot, box plots were built grouping the data per well, and confirm the trends described above (Figure 11). The $\delta^{18}O$ of shells increases significantly upward through the formation, whereas this increase is strongly attenuated in the bulk rock signal, and noticeable mostly between EST1203 and EST-1201. The shell $\delta^{13}C$ values are similar in the 3 wells, whereas the bulk values show a slight but clear decrease from base to top.

Porosity and permeability

Porosity and permeability data are characteristics of microporous carbonates and fit with the classical fields of data of microporous oil and gas reservoirs (Lucia, 2007; Lonoy, 2016; Ehrenberg, 2019). The large dominance of mud-supported mudstone to wackestone textures, and more rarely packstone, is in line with the dataset. Porosity can reach up to 27% but permeability rarely exceeds 1mD, with only 7 values above this threshold over a total of 123 measurements (Figure 12). The latter higher permeability values always correspond to specific levels or samples, either (1) located in the grainstone of the "Oolithe de Bure" Member which shows some preserved cement-reduced interparticle/mouldic pores (Figure 6), or (2) showing intra-sample discontinuities such as microfractures or stylolites re-opened during the permeability measurement.

Porosity values slightly increase upward through the "Calcaires du Barrois" Formation, showing a net positive kick above 75m and the boundary between the "Calcaires de Dommartin inférieurs", and "Calcaires de Dommartin médians" sub-members (Figure 4). Permeability data do not show the same trend although the values exceeding 0.1mD are statistically more abundant in the EST-1201 well, even excluding the values of the "Oolithe de Bure". The other values above 1mD are located lower in the formation, in the two lowermost members, and correspond to samples with internal heterogeneities (Pellenard et al., 2011). The stratigraphic upward increase of porosity is confirmed by box plots (Figure 13). Permeability on the contrary does not show significant change between EST-1218 and EST-1203, but increases up significantly between the latter and EST-1201. Box plots show that this increase is not only linked to the high permeability outliers within the "Oolithe de Bure".

Mechanical properties

The density of data is higher in the lower part of the formation because of its higher homogeneity. In the upper part, within the uppermost members, the intensity of bioturbation, enhanced by karst (Figure 9), and the overall increasing alteration of cores did not allow a highly continuous record of the Schmidt hammer.

Young's Modulus E values decrease from the base to the top of the "Calcaires du Barrois" Formation, although the EST-1203 and EST-1201 wells show a significant range of variation (Figure 4; Figure 14). An overall differential impact of burial compaction between the base and the top of the formation on the E values is excluded considering its limited thickness of a maximum of 140m. The lowest values are recorded in the underlying marls of the "Marnes à exogyres" Formation, and as well in the "Oolithe de Bure" Member. Consequently, the two parameters influencing E values are clay content and porosity. XRD dataset being not dense enough, the GR signal, mostly dependent on clay content here, was discretised by only considering the data in a window of ±20cm around a value of E. In the lower half of the formation, up to 75m approximately, there is a direct opposite relationship between E and GR, thus clay content (Figure 14). Above, the two signals dissociate and are positively correlated in a few intervals (70-60m, 42.5-35m).

Discussion

Characterisation of an eogenetic and a telogenetic meteoric diagenesis

The dissociation between the $\delta^{18}O$ and $\delta^{13}C$ signals of shells and bulk rocks through the formation is the result of the diagenetic alteration of micrites. A recrystallisation of micrites synchronously during the precipitation of burial cements, such as the ones present in the grainstone of the "Oolithe de Bure", would explain some depletion of the bulk values compared to shells. However, the increased upward divergence between bulk and shell $\delta^{18}O$ values (Figure 4; Figure 11) indicates a stratigraphic partitioning of the diagenetic alteration. Also, such a recrystallisation would not explain the decreasing upward trend of the $\delta^{13}C$ of micrite observed through the formation. A more likely explanation is that the stable isotope trends illustrate the effects of an early diagenesis linked to long-lasting subaerial exposures that occurred at the Jurassic-Cretaceous transition (Brigaud et al., 2018). This set of events led to the occurrence of a major discontinuity in the well EST-1201 at 15m. The development of a karst, of soil horizons, and the flow of freshwaters in the underlying limestone of the "Calcaires du Barrois" easily explain the patterns of the isotopic signals. The micrites were mineralogically stabilised (high magnesian calcite or HMC, to low magnesian calcite or LMC, aragonite dissolution or neomorphism to calcite) and recrystallised (Brigaud et al., 2014; Hashim and Kaczmareck, 2019; and references therein) during these flows of freshwater charged in light C from surface soils (e.g. Allen and Matthews, 1982; Immenhauser et al., 2008). Such an early diagenesis does not fully exclude the possibility that some recrystallisation also affected the micrites during burial.

The bulk $\delta^{13}C$ curves of the 3 wells, non-concatenated and with their original depths, reveals a very similar evolution of decreasing upward values (Figure 15). In the wells EST-1218 and EST-1203, the trend is similar to the overall trend observed through the formation (Figure 4). Moreover, in the lower parts of these 2 wells, shell and bulk $\delta^{13}C$ values are overlapping, but are clearly diverging in the upper 20-30m (Figure 15). In the EST-1201 well, the decrease of bulk $\delta^{13}C$ values is also visible despite less pronounced, but the separation with the shell values is clear. It must be noted here that the "Calcaire du Barrois" Formation is not at the surface in this well, covered by 15m of early Cretaceous deposits. This common evolution is recorded in distinct members of the formation in the 3 wells. It definitely illustrates the effect of a recent Cenozoic telogenetic diagenesis, linked to the return of the studied limestone to the surface, implying again some recrystallisation through the flow of freshwater charged in light C, but certainly far more limited than during the early Cretaceous exposures.

The interval of overlap between the wells EST-1203 and EST-1201 is of particular interest here. This interval concerns the sub-members of the "Calcaires de Dommartin médians" and "Calcaires de Dommartin supérieurs", between 0m and 17.5m in EST-1203 and between 41m and 60m in EST-1201. In this overlap, the bulk $\delta^{18}O$ values are very similar in terms of absolute values and vertical evolution in the 2 wells (Figure 16). The bulk $\delta^{13}C$ values show the same decreasing upward trend but are systematically lower (by about 0.5‰) in EST-1203, where the succession is close to the surface, than in EST-1201 where the succession is slightly deeper (Figure 16). This is another demonstration of the effect of the recent telogenetic diagenesis.

In summary, the isotopic signals illustrate the cumulated impact of two distinct episodes of surface diagenesis. The first is early and associated to the subaerial exposures linked to the unconformities at the Jurassic-Cretaceous transition, and the second is recent and linked to the return to the surface of the "Calcaires du Barrois" during the Cenozoic after a burial phase in the late Cretaceous. These two stages of diagenesis and carbonate cementation have been clearly dated by in situ U-Pb geochronology in the area (Pagel et al., 2018; Brigaud et al., 2020; Blaise et al., 2022). These stages are associated with major deformation phases at the western European lithospheric scale: (1) the Bay of Biscay rifting (Late Jurassic–Early Cretaceous), and (2) Eocene north-south Pyrenean compression followed by Oligocene east-west extension during the West European Cenozoic rifting (Brigaud et al., 2020).

The impact of the eogenetic diagenesis is almost invisible below the "Calcaires de Dommartin inférieurs" sub-member, micrites showing almost the same isotopic signal as the LMC shells (within 1‰ median difference for both $\delta^{18}O$ and $\delta^{13}C$; Figure 13), which is not following some findings of

Hasiuk et al. (2016) who reported consistent shifts of a few per mil between $\delta^{18}O$ compositions of LMC microcrystals and age equivalent marine calcites.

The impact of the recent telogenesis is slightly less recorded at the top of EST1218 (Figure 16) than in the other two wells because the members that are close to the surface in that well, i.e. the "Pierre châline" and the "Calcaires de Dommartin inférieurs", are significantly more argillaceous. The flow of meteoric waters was lower and slower than in the upper members (the "Pierre châline" is an aquitard).

Impact of the 2-stages meteoric diagenesis on the petrophysical properties of micrites

The early mineralogical stabilisation is also known to preserve the microporosity of micrites (Carpentier et al., 2015; Hashim and Kaczmareck, 2019; Vincent et al., 2020 and references therein), with, however, a significant re-arrangement of the nano/micro-pore structures (Lucia and Loucks, 2013); micrites then show subhedral to euhedral textures of Types I and II *sensu* Kaczmarek et al. (2015). However, long-lasted exposures under favourable climates can sometimes lead to more intense recrystallisation of micrites under karstic surfaces (Vincent et al., 2019), where they show coarser dense anhedral and coalescing textures of Type III *sensu* Kaczmarek et al. (2015). In the present case study, the upper part of the palaeokarst linked to the unconformity of the Jurassic-Cretaceous transition has likely been eroded since Valanginian clastic sediments directly rest on an incomplete "Calcaires cariés et Calcaires tachetés" Member. The overall increase upward of porosity through the "Calcaires du Barrois" Formation illustrates the impact of the meteoric diagenesis linked to the subaerial exposures during the Jurassic-Cretaceous unconformities. The lower part of the formation below the "Calcaires de Dommartin inférieurs" sub-member, where porosity remains low, was less to non-affected by early meteoric diagenesis because (1) it was farther from the surface, and (2) it is overall more argillaceous, which prevented from efficient flows of freshwater. Meteoric diagenesis does not seem to be mandatory for the development of mineralogical stabilisation, but nevertheless seems to promote and/or emphasize the process (see discussion in Hashim and Kaczmareck, 2019). Thus, early mineralogical stabilisation was most likely less efficient in this lower part of the formation, and reversely, chemical compaction during burial was more intense with clays acting as probable catalysers (Lambert et al., 2006; Ehrenberg, 2004), which is confirmed by a higher intensity of stylolites is this lower interval (Figure 14). Microporosity was not preserved because, despite mineralogical stabilisation probably having occurred during the early stages of burial (Hashim and Kaczmareck, 2019), it was followed by an increase of micrite crystal size. This occurred through overgrowths or cementation of crystals together (Lucia, 2017), leading to their coalescence, and to the observed fitted textures of Type III *sensu* Kaczmarek et al. (2015). Dissolved carbonate

was sourced locally by pressure-dissolution, and the slight depletion of $\delta^{18}O$ values of micrites compared to LMC shells probably reflects the slightly higher temperatures during these cementations.

The S48 ratio also evolves upward with an overall decrease mostly recorded along EST-1203 (Figure 17). This trend clearly results from the above mentioned upward change in the micrite fabric, and of the pore network through the formation, despite microporosity is the largely dominant pore-type. In the lower part, all the porosity is accessible by simple imbibition of water which is consistent with small pores between clustered to fitted crystals. In the upper part, only part of the porosity is invaded by simple imbibition, air bubbles being trapped in the core of slightly larger pores during imbibition, which is consistent with the upward evolution of the micrite textures showing more loosely packed subhedral crystals. The inverse relationship between pore-throat/pore size and crystals size within micrite textures (Kaczmarek et al., 2015) explains this phenomenon. Moulds (macro and micro) of former aragonite elements are observed in the upper part of the formation, mouldic dissolution having been most likely amplified upward during the subaerial exposures of the Jurassic-Cretaceous transition. These isolated pores may also participate to the upward decrease of S48. Identifying the initial mineralogical precursor of the studied micrites is beyond the scope of this work. But it is likely that despite the fact that there is an evolution of the faunal assemblages through the "Calcaires du Barrois Formation", the precursor sediment at the origin of micrites remained the same, dominated by an assemblage of aragonite and HMC (e.g. Hashim and Kaczmareck, 2019). Therefore, the vertical evolution of micrite textures and associated petrophysical properties reflects a stratigraphically differentiated diagenesis affecting similar initial precursors.

The recent Cenozoic telogenesis also has an impact, although less pronounced, on the petrophysical properties. Within the interval of overlap between the wells EST-1203 and EST-1201, porosity values are systematically lower in EST-1203, where the "Calcaires de Dommartin" are closer to the surface, than in EST-1201 (Figure 18). Permeability values are also lower in EST-1203 than in EST-1201, although remaining in the same order of magnitude (Figure 18). It is most likely that the calcite dissolved at the surface reprecipitated-s slightly deeper, probably preferentially as cements in the largest pores such as moulds, preserving the microporosity in micrites (e.g. Ehrenberg and Walderhaug, 2015).

It is worth noting that the S48 ratio is showing a decreasing-upward trend in each well separately, on top of the overall decrease through the formation (Figure 17). This is another demonstration of the stacked impacts of the eogenetic and telogenetic meteoric diagenesis on the micrite properties. This

individual decrease is however less pronounced in EST-1218 than in the other 2 wells, because the outcropping members in this well are more argillaceous and suffered a distinct burial diagenesis.

Resulting impacts on the mechanical properties

As already stated, it is clear that clay content negatively impacts Young's Modulus E values. In the "Calcaires sublithographiques" and "Pierre châline" Members and the "Calcaires de Dommartin inférieurs" sub-member, below 75m, argillaceous limestones show the lowest E values and the cleanest limestones show the highest E values of the entire studied interval (Figure 14). The negative relationship between E and clay content, illustrated by GR values, is clear despite a low R^2 of 0.41 for the linear regression (Figure 19). In this interval, the cleanest limestones are also less porous (Figure 20). The levels showing porosity higher than 10% form an out of trend cloud (Figure 20), but as already stated samples with moderate porosity and permeability in that lower part of the formation may have internal heterogeneities. This lower part of the "Calcaires du Barrois" Formation did not or underwent far less the early diagenesis linked to the exposures of the Jurassic-Cretaceous transition. Chemical compaction was there pronounced and micrites recrystallised and became dense and tight (aggrading neomorphism *sensu* Folk, 1965). Fracture intensity in this lower half of the formation is significant (Figure 14).

Above 75m, the formation is overall less argillaceous, except very localised interbeds, and above 45m porosity has a greater negative impact on mechanical properties. The macroporous clean grainstones of the "Oolithe de Bure" show the lowest E values of the succession (Figure 14). The uppermost part of the formation also consisting of clean limestone but microporous, also shows low E values. The number of points available after GR discretisation is however too low to properly illustrate trends on cross-plots (Figure 19; Figure 20). The upper part of the formation, above the "Oolithe de Bure" is less fractured than the other intervals.

In between 45m and 75m, relationships are less obvious in a zone showing thin alterations between clean limestones and slightly argillaceous limestones in the upper parts of the "Calcaires de Dommartin médians" and "Calcaires de Dommartin supérieurs" sub-members. The latter sub-members show the highest intensity of fractures (Figure 14) which may have affected the Schmidt hammer rebound measurements.

Implication for the understanding of the aquifer architecture of the "Calcaires du Barrois"

All the preceding results and discussions lead to the identification of a significant intra-formation boundary sitting around the depth 75m, which corresponds to the boundary between the "Calcaires de Dommartin inférieurs" and the "Calcaires de Dommartin médians" sub-members.

The limestones situated above this boundary are clean with a low clay content. During the long-lasted exposures associated with the unconformities of the Jurassic-Cretaceous transition, karst and soils developed on top of these. Freshwaters penetrated down into this upper part of the "Calcaires du Barrois" Formation, leading to mineralogical stabilisation and preservation of microporosity within micrites that did not evolve much later during mesogenesis (Figure 21). The only grainy level of the "Oolithe de Bure" underwent the same eogenesis but was also partially cemented by calcite burial cements. The limestone located below this boundary are overall more argillaceous, also showing some bioclastic marly beds. The early freshwater downflows did not reach these levels, or had a very minor impact, limiting the mineralogical stabilisation. Together with the presence of clays within micrites, this explains that a significant chemical compaction affected the lower part of the formation during the burial phase of the late Cretaceous. Local redistribution of dissolved carbonates and incomes of fluids from the clay-rich layers led to an intense recrystallisation and cementation of the micrites (Figure 21).

The return to the surface of the formation during the Cenozoic did not modify in depth the previously acquired properties. Only the upper members, less argillaceous than the lower ones, were slightly affected by dissolution-reprecipitation processes linked to the surficial (10m maximum) flow of recent freshwaters (Figure 22). In the lower members, only the vicinity of microfractures evidences recent dissolutions linked to the flow of freshwaters.

As a result, the lower members of the formation below the 75m boundary are dense, tight, with low matrix permeability to non-permeable, and are showing microfractures in limestone, open or partially cemented by calcite cement. The micritic limestones there show high Young's Modulus E values. The upper members above the boundary are microporous, show low to locally moderate matrix permeability, and the micritic limestones show low Young's Modulus E values, with a faint decreasing-up trend. Microfractures are here rare in limestone. The "Oolithe de Bure" Member is a thin interval with high porosity and possibly permeability, and very low Young's Modulus E values. The "Calcaires de Dommartin médians" and "Calcaires de Dommartin supérieurs" sub-members are the most intensively fractured. They are located between the intra-formational boundary at 75m and the "Oolithe de Bure" Member, in a diagenetic and petrophysical transitional stratigraphic interval. Consequently, they likely accommodated most of the deformation linked to the Pyrenean and Alpine orogens of the Cenozoic.

The above findings shed a new light on the knowledge of the "Calcaire du Barrois" karstic aquifer. The recharge zone of the later corresponds to the outcrop of the formation, where the ZIDS is located (Figure 1). The hydrologic karst network then develops under cover towards the Northwest,

below the Purbeckian and Lower Cretaceous series (Jaillet, 2005). The current hydrogeological conceptual model divides the aquifer in two sub-aquifers: a lower captive sub-aquifer within the "Calcaires sublithographiques" Member, and an upper free sub-aquifer encompassing all the members above the "Pierre châline", the latter being a boundary aquitard (Figure 23).

It is now clear that the flow in the lower captive sub-aquifer is driven by hydraulic conductivity of the microfracture network, the matrix properties being very low. This sub-aquifer does not develop a mature karst with cavities downstream (Jaillet, 2005). The upper free sub-aquifer, currently considered as a single system with a unique behaviour (Andra, 2022), shall in fact be split into several sub-zones. The lower part up to the intra-formational boundary consists of the "Calcaires de Dommartin inférieurs", which displays petrophysical and mechanical properties very similar to the "Calcaires sublithographiques". Consequently, it most probably displays a similar hydraulic behaviour to the lower captive aquifer, with microfractures being key to the hydraulic conductivity. The intensively fractured "Calcaires de Dommartin médians" and "Calcaires de Dommartin supérieurs" interval, between the intra-formational boundary and the "Oolithe de Bure" is the zone with the highest vertical and possibly lateral hydraulic conductivity. Not only microfractures may participate but also matrix, especially in the upper part. Outcrops of that particular interval are probably the main recharging areas of the upper free sub-aquifer. Jaillet (2005) indicates that the vertical conducts of the mature karst system under cover stop at the "Pierre châline", and that the main horizontal bottom drainages occur at that level. Jaillet (2005) positioned the "Pierre châline" at the first slightly argillaceous level from top to bottom in the succession. However, according to the more recent wells drilled in the area including the 3 wells studied here, it appears that what he interpreted as the top of the "Pierre châline" corresponds to the first significant GR peak at the top of the "Calcaires de Dommartin inférieurs" (Figure 2; Figure 3). Therefore, the critical hydraulic boundary is not the "Pierre châline" but the intra-formational boundary (Figure 23), sitting approximately 25m above.

The "Oolithe de Bure" is currently considered as an aquitard within the upper free sub-aquifer (Andra, 2022). The fact that it may be considered as a hydraulically specific level cannot be discussed, but the new petrographic and petrophysical results seem to show a significant aquifer potential in this thin Member. It would be interesting to see if flows are channelised on top of it or within it.

Finally, the uppermost zone of the upper free sub-aquifer behaves in its own way. Fractures are rare and barely participate to the hydraulic conductivity. Flows are channelized in networks of burrows,

which is a starting point for the development of more mature features downstream, and matrix also certainly participates to a certain extent.

Conclusions

The “Calcaires du Barrois” limestone Formation of late Kimmeridgian to early Tithonian age, and outcropping in the Eastern edge of the Paris Basin, is an active karstic aquifer. The Zone of Interest for Detailed Surveys (ZIDS) defined by the Andra (French National Agency for Radioactive Waste Management) for the potential deep repository site for radioactive wastes is located within the recharge zone of this aquifer. In order to better understand the aquifer characteristics, three reference cored wells EST-1201, EST-1203, and EST-1218, located within the ZIDS and cutting through the “Calcaires du Barrois”, were studied with a multidisciplinary approach, integrating petrography, C & O stable isotope geochemistry, XRD analyses, petrophysics and geomechanics.

Largely dominated by mud-supported micritic textures, the “Calcaires du Barrois” is a 140m-thick Formation composed of eight Members and sub-members, and only shows a thin interval of grainstone in its upper half, corresponding to the “Oolithe de Bure” Member. Several stages of diagenesis affected these limestones modifying in depth their primary properties.

An early (eogenetic) critical stage of meteoric diagenesis was associated with a set of unconformities and long-lasted subaerial exposures at the Jurassic-Cretaceous transition, when karst and soils developed on top of the formation as identified by stable isotopes. Downflows of freshwater penetrated the upper half of the formation, mostly showing clean clay-poor limestones with some aragonitic components, and mineralogical stabilisation, among other processes, allowed to preserve efficiently microporosity in micrites, which show subhedral to euhedral textures. The lower half of the formation, showing more argillaceous facies and a few marly beds with dominantly calcitic components, was less to non-affected by the freshwater flows. There, burial diagenesis (mesogenesis) has been active and especially chemical compaction, leading to recrystallisation and cementation of micrites, which became tight showing subhedral clustered to anhedral fitted textures. In the upper half of the “Calcaires du Barrois”, burial diagenesis had a limited impact, with probably only limited cementation in the grainstone interval, remaining macroporous. More recently, the Cenozoic Pyrenean and Alpine orogens led to the return to the surface of the formation. Whatever the member outcropping nowadays, recrystallisation affected the micrites in a thin pluri-metre thick surficial zone, but this recent diagenesis did not affect significantly the previously acquired properties.

This multi-stage diagenesis progressively created an intra-formational boundary within its middle part (75m), which is critical because defining distinct mechanical and petrophysical zones. Below this boundary, micritic limestones are tight with high Young's Modulus E values, and show a moderate intensity of fractures. Above the boundary, micritic limestones are microporous with low Young's Modulus E values, and show almost no fractures. There is a transitional interval between this intra-formational boundary and the macroporous "Oolithe de Bure" Member, which accommodated most of the Cenozoic deformation and where microporous micritic limestones are very intensively fractures.

This high-resolution characterization of the "Calcaires du Barrois" Formation provides a conceptual model explaining the stratigraphic distribution of mechanical and petrophysical properties of micritic limestones, guided by the interplay of sedimentology and diagenesis. This leads to distinguish in the study area: (1) an upper microporous interval with an intensively fractured lower layer favourable to the freshwater flows, and linked to a mature karst system under cover in a downstream location to the Northwest, and (2) a lower tight interval with a much lower hydraulic conductivity driven by microfractures, and which does not evolve downstream in a mature karst system, flow rates and conducts being both limited. The current hydrogeological model considers a purely sedimentological boundary to delimit the two intervals, but shall be reappraised since it is here demonstrated that the boundary is located 25m higher and is inherited from a multi-stage diagenesis. These are critical elements that will complement and influence the works on the conception of industrial facilites at surface and shallow subsurface for the CIGEO project.

More broadly, such an integrated detailed study reminds the need of better characterising micritic limestones that are often considered, and very often wrongly, as sedimentological and diagenetic homogeneous series.

Acknowledgement

We would like to thank the Andra for the support to the technical project and overall, for giving the authorization to publish the results. Our warm thanks also go to Philippe Blanc (Lithologie Bourgogne) for the sample preparation, and to Emilie Steimetz from the Laboratoire Biogéosciences of the University of Burgundy for having operated the SEM session. This manuscript benefitted greatly from the reviews by Jonathan Turner and Alun Williams, but also from the thorough editing work by Paul Wright.

References

AISSAOUI, D.M., 1988. Magnesian calcite cements and their diagenesis: dissolution and dolomitisation, Mururoa Atoll. Sedimentology 35, 821–841.

ALLEN, J.R., and MATTHEWS, R.K., 1982. Isotope signatures associated with early meteoric diagenesis. Sedimentology, 29, 797-817.

ANDRA, 2022. Dossier d'Autorisation de Création (DAC – Construction Licence Application) de l'installation nucléaire de base (INB) Cigéo ; Pièce 6 : étude d'impact du projet global Cigéo – Volume 3 : Etat actuel de l'environnement et facteurs susceptibles d'être affectés par le projet ; Chapitres 1 à 5. CG-TE-D-EDM-AMOA-ESE-0000-22-0005/A. https://www.andra.fr/sites/default/files/2023-04/Pi%C3%A8ce%2006-Etude%20impact-Vol3-Etat%20actuel-Chapitres%201-5.pdf

ANDRE, G., HIBSCH, C., FOURCADE, S., CATHELINEAU, M., and BUSCHAERT, S., 2010. Chronology of fracture sealing under a meteoric fluid environment: Microtectonic and isotopic evidence of major Cainozoic events in the eastern Paris Basin (France). Tectonophysics 490, 214–228.

ANDRE, G., PROUDHON, B., REBOURS, H., and WILEVEAU, Y., 2006. Paramètres contrôlant la distribution de la fracturation : exemple dans une série marno-calcaire du Jurassique supérieur (Est du bassin de Paris). Comptes Rendus Geoscience, Le Callovo-Oxfordien du bassin de Paris : du contexte géologique à la modélisation de ses propriétés 338, 931–941.

BLAISE, T., ALI KHOUDJA, SA., CARPENTIER, C., BRIGAUD, B., MISSENARD, Y., MANGENOT, X., BOULVAIS, P., LANDREIN, P., And COCHARD, J., 2022. Far-field brittle deformation record in the eastern Paris Basin (France). Geological Magazine, 159, 2095-2109.

BLAISE, T., BARBARAND, J., KARS, M., PLOQUIN, F., AUBOURG, C., BRIGAUD, B., CATHELINEAU, M., EL ALBANI, A., GAUTHERON, C., IZART, A., JANOTS, D., MICHELS, R., PAGEL, M., POZZI, J-P., BOIRON, M-C., and LANDREIN, P., 2014. Reconstruction of low burial (< 100 °C) in sedimentary basins: A comparison of geothermometer sensitivity in the intracontinental Paris Basin. Marine and Petroleum Geology, 53, 71-87.

BRIGAUD, B., BONIFACIE, M., PAGEL, M., BLAISE, T., CALMELS, D., HAURINE, F., and LANDREIN, P., 2020. Past hot fluid flows in limestones detected by Δ47–(U-Pb) and not recorded by other geothermometers. Geology, 48, 851-856.

BRIGAUD, B., VINCENT, B., PAGEL, M., GRAS, A., NORET, A., LANDREIN, P., and HURET, E., 2018. Sedimentary architecture, depositional facies and diagenetic response to intracratonic deformation

and climate change inferred from outcrops for a pivotal period (Jurassic/Cretaceous boundary, Paris Basin, France). Sedimentary Geology, 373, 48-76.

BRIGAUD, B., VINCENT, B., CARPENTIER, C., ROBIN, C., GUILLOCHEAU, F., YVEN, B., and HURET, E., 2014. Growth and demise of the Jurassic carbonate platform in the intracratonic Paris Basin (France : interplay of climate change, eustasy and tectonics. Marine and Petroleum Geology, 53, 3-29.

BRIGAUD, B., DURLET, C., DECONINCK, J.F., VINCENT, B., THIERRY, J., and TROUILLER, A., 2008. The origin and timing of multiphase cementation in carbonates: impact of regional scale and geodynamic events on the Middle Jurassic limestone diagenesis (Paris Basin, France). Sed. Geol., 222, 161-180.

BURCHETTE T, AND WRIGHT VP, 1992. Carbonate ramp depositional systems. Sed. Geol., 79, 3–57.

CARPENTIER, C., FERRY, S., LECUYER, C., STRASSER, A., GERAUD, Y. AND TROUILLER, A., 2015. Origin of micropores in late Jurassic (Oxfordian) micrites of the Eastern Paris Basin, France. J. Sed. Res., 85, 660-682.

COLLECTIF SERVICE DRD/MG, 2011. Projet HA/MA-VL - La formation du Barrois - Etat des connaissances et apport des reconnaissances 2010 sur la ZIRA. ANDRA Report, N° D.RP.ASMG.11.0044, 55p.

DEVILLE DE PERIERE, M., DURLET, C., VENNIN, E., CALINE, B., BOICHARD, R., and MEYER, A., 2017. Influence of a major exposure surface on the development of microporous micritic limestones - Example of the Upper Mishrif Formation (Cenomanian) of the Middle East. Sedimentary Geology 353, 96–113.

DEVILLE DE PERIERE, M., DURLET, C., VENNIN, E., LAMBERT, L., BOURILLOT, R., CALINE, B., and POLI, E., 2011. Morphometry of micrite particles in cretaceous microporous limestones of the Middle East: Influence on reservoir properties. Marine and Petroleum Geology 28, 1727–1750.

EHRENBERG, S.N., 2019. Petrophysical heterogeneity in a lower Cretaceous limestone reservoir, onshore Abu Dhabi, United Arab Emirates. AAPG Bull., 103, 3, 527-546.

EHRENBERG, S.N., 2004. Factors controlling porosity in the Upper Carboniferous-Lower Permian carbonate strata of the Barents Sea. AAPG Bull., 88, 12, 1653-1676.

EHRENBERG, S.N. and WALDERHAUG, O., 2015. Preferential calcite cementation of macropores in microporous limestones. J. Sed. Res., 85, 780-793.

FOLK, R.L., 1965. Some aspects of recrystallization in ancient limestones. In: L.C. Pray and R.C. Murray (Eds), Dolomitisation and limestone diagenesis: a symposium. SEPM Spec. Pub., 13, 14-48.

HARMAND, D., LEJEUNE, O., JAILLET, S., ALLOUC, J., OCCHIETTI, S., BRULHET, J., FAUVEL, P-J., HAMELIN, B., LAURAIN, M., LE ROUX, J., MARRE, A., PONS-BRANCHU, E., QUINIF, Y., AND DEVOS, A., 2004. Dynamique de l'érosion dans le Barrois et le Perthois (Est du Bassin de Paris) : incision et karstification dans les bassins-versants de la Marne, de la Saulx et de l'Ornain. Quaternaire, 15 (4), 305-318.

HASIUK, F.J., KACZMAREK, S.E., AND FULLMER, S.M., 2016. Diagenetic origins of the calcite microcrystals that host microporosity in limestone reservoirs. J. Sediment. Res. 86 (10), 1163–1178.

HASHIM, M., AND KACZMAREK, S., 2019. A review of the nature and origin of limestone microporosity. Marine and Petroleum Geology, 107, 527-554.

IMMENHAUSER, A., HOLMDEN, C, & PATTERSON, W.P., 2008. Interpreting the carbon isotope record of ancient shallow epeiric seas: Lessons from the Recent. In B.R. Pratt and C. Holmden (Eds.) "Dynamics of Epeiric Seas", Geological Association of Canada Special Publication, p. 135-174.

JACQUIN, T., DARDEAU, G., DURLET, C., DE GRACIANSKY, C., and HANTZPERGUE, P., 1998. The North Sea cycle: an overview of 2nd-order transgressive/regressive facies cycles in western Europe. In: de Graciansky, P.-C., Hardenbol, J., Jacquin, T., Vail, P.R. (Eds.), Mesozoic and Cenozoic Sequence Stratigraphy of European Basins. SEPM Special publication No. 60, pp. 445–466.

JAILLET, S.,2005. Le Barrois et son karst couvert, Structure, Fonctionnement, Évolution. Karstologia Mémoires, 12, PhD. University of Bordeaux 3, 336 p.

KACZMAREK, S.E., FULLMER, S.M. and HASIUK, F.J., 2015. A universal classification scheme for the microcrystals that host limestone microporosity. J. Sed. Res., 85, 1197-1212.

LAMBERT, L., DURLET, C., LOREAU, J.-P., and MARNIER, G., 2006. Burial dissolution of micrite in Middle East carbonate reservoirs (Jurassic–Cretaceous): keys for recognition and timing. Marine and Petroleum Geology 23, 79–92.

LANDREIN, P., VIGNERON, G., DELAY, J., LEBON, P., and PAGEL, M., 2013. Lithologie, hydrodynamisme et thermicité dans le système sédimentaire multicouches recoupé par les forages Andra de Montiers-sur-Saulx (Meuse). Bull. Soc. Géol. France, 184, 6, 519-543.

LINARD, Y., VINSOT, A., VINCENT, B., DELAY, J., WECHNER, S., De La VAISSIERE, R., SCHOLZ, E., GARRY, B., LUNDY, M., CRUCHAUDET, M., DEWONCK, S., and VIGNERON, G., 2011. Water flow in the

Oxfordian and Dogger limestone around the Meuse/Haute-Marne Underground Research Laboratory. Physics and Chemistry of the Earth, 36, 1450-1468.

LINDHOLM, R.C., and FINKELMAN, R.B., 1972. Calcite staining: semiquantitative determination of ferrous iron. J. Sed. Petrol., 42, 239-242.

LONOY, A., 2016. Making sense of carbonate pore systems. AAPG Bull., 90, 9, 1381-1405.

LUCIA, J.F., 2007. Carbonate Reservoir Characterization. Springer-Verlag.

LUCIA, J.F., 2017. Observations on the origin of micrite crystals. Marine and Petroleum Geology, 86, 823-833.

LUCIA, J.F., AND LOUCKS R.G., 2013. Micropores in carbonate mud: early development and petrophysics. GCAGS journal, 2, 1-10.

LOREAU J.P., 1972. Pétrographie des calcaires fins au microscope électronique à balayage : introduction à une classification des "micrites". C. R. Acad. Sci. Paris, 274, 810-813.

MEGNIEN, C., AND MEGNIEN, F., 1980. Synthèse géologique du Bassin de Paris. BRGM Mem. 101, 446 pp.

MERTZ J.D., (1991). Structures de porosité et propriétés de transport dans les grés. Sci. géol. Mém. 90, 149p.

MOREAU, K., BRIGAUD, B., ANDRIEU, S., BRIAIS, J., HAURINE, F., BLAISE, T., AND QESNEL, F., 2023. Caractérisation de processus diagénétiques par la datation in-situ U–Pb de ciments de calcite : exemple de la karstification dans les calcaires du Cénozoïque du Bassin de Paris. 28th Earth Science Meeting, Rennes, 30/10-03-11, sciencesconf.org:rst2023-rennes:484893.

MOSHIER S.O., 1989. Microporosity in micritic limestones: a review. Sed. Geol., 63, 191-213.

MUNNECKE, A., WRIGHT, V.P., AND NOHL, T., 2023. The origins and transformation of carbonate mud during early marine burial diagenesis and the fate of aragonite: A stratigraphic sedimentological perspective. Earth Science Reviews, 239, doi.org/10.1016/j.earscirev.2023.104366.

PELLENARD, P., GIGOUX, M., REGNET, J.-B., DURLET, C., PUCEAT, E., RICHARD, J., and SIZUN, J.-P., 2011. Caractérisation des propriétés pétrophysiques, minéralogiques et géochimiques des calcaires du Kimméridgien-Tithonien (Calcaires du Barrois) de la ZIRA. ANDRA Report, N° D.RP.0UNB.11.0001, 114p.

REGNET, J.B., DAVID, C., ROBION, P., and MENÉNDEZ, B., 2019. Microstructures and physical properties in carbonate rocks: A comprehensive review. Marine and Petroleum Geology 103, 366–376.

REGNET, J-B., ROBION, P., DAVID, C., FORTIN, J., BRIGAUD, B., and YVEN, B., 2015. Acoustic and reservoir properties of microporous carbonate rocks: implication of micrite particle size and morphology. Journal of Geophysical Research. Solid Earth, 120, 790-811.

REZAK, R., and LAVOIE, D.L., 1993. Carbonate microfabrics. Springer-Verlag, 313p.

RICHARD, J., SIZUN, J.P., and MACHHOUR, L., 2007. Development and compartmentalization of chalky carbonate reservoirs: the Urgonian Jura–Bas Dauphine platform model (Genissiat, southeastern France). Sedimentary Geology, v. 198, p.195–207.

SMITH, L., 2023. Fitted fabric grainstones – a common product of subaerial exposure and vadose diagenesis. 17th Bathurst Meeting, Naples, Italy, 5-7 September 2023.

VINCENT, B., AL-ZANKAWI, O., HAYAT, L., GARLAND, J., GUTTERIDGE, P., and THOMPSON, S., 2020. Unravelling the complexity of thin (sub-seismic) heterogeneous carbonate reservoirs: an integrated study of the Albian Mauddud Formation in the Greater Burgan area, Kuwait. J. Petrol. Geol., 43 (3), 249-276.

VINCENT, B., WITKOWSKI, F., HORBURY, A., CHISTYAKOV, A., KOLOSKOV, V. and DMITRIEV, S., 2019. Depositional and diagenetic controls of carbonate reservoir property distribution in a Super Giant reservoir, SE Iraq. 1st EAGE Workshop in Characterisation and workflows for giant carbonate fields, 17-21 February, Abu Dhabi.

VINCENT, B., EMMANUEL, L., HOUEL, P., and LOREAU, J.P., 2007. Geodynamic control on carbonate diagenesis: petrographic and isotopic investigation of the Upper Jurassic Formations of the Paris Basin (France). Sed. Geol., 197, 267-289.

VOLERY, C., DAVAUD, E., DURLET, C., CLAVEL, B., CHAROLLAIS, J., and CALINE, B.. 2010, Microporous and tight limestones in the Urgonian Formation (late Hauterivian to early Aptian) of the French Jura Mountains: focus on the factors controlling the formation of microporous facies. Sedimentary Geology, v. 230, p. 21–34.

VOLERY, C., DAVAUD, E., FOUBERT, A., and CALINE, B., 2009. Shallow-marine microporous carbonate reservoir rocks in the Middle East: relationship with seawater Mg/Ca ratio and eustatic sea level. Journal of Petroleum Geology, v. 32, p. 313–325.

WESTPHAL, H., MUNNECKE, A., BOHM, F., AND, BORNHOLDT, S., 2008. Limestone-marl alternations in epeiric sea settings – witnesses of environmental changes or diagenesis?. Geological Association of Canada Special Paper 48, 389-406.

ZINSZNER, B., and PELLERIN, F.-M., 2007. Geoscientists Guide to Petrophysics. Editions Technips, Paris.

Figure Captions

Figure 1: (A) Broad structural map of Northeast France showing the main regional tectonic elements and the study area (red square). (B) simplified geological map of the study area with the location of the ZIDS (Zone of Interest for Detailed Surveys, black square) and the 3 studied cored studied wells, and the Andra URL (Underground Research Laboratory; red asterisks).

Figure 2: Simplified sedimentological log of the Late Kimmeridgian to Valanginian succession outcropping in the study area reconstructed from the integration of the 3 reference wells (see Figure 3); the "Calcaires du Barrois" Formation is subdivided in 8 Members and sub-members.

Figure 3: (A) Individual GR traces along each reference well from ground surface (KB); note the overlap interval between wells EST-1201 and EST-1203. (B) Concatenated GR traces of the 3 wells forming a continuous record through the "Calcaires du Barrois" Formation (used on Figure 2); note that late Tithonian and Berriasian deposits are absent in EST-1201 where Valanginian clastics are resting on the "Caclaires du Barrois" forming an unconformity at 15m approximately.

Figure 4: Compilation of all the acquired results for XRD, porosity and permeability, Young's Moudulus (see the text for explanation of calculations), and C & O stable isotopes along the reference GR concatenated trace. Porosity and permeability data are complemented by data from Pellenard et al. (2011). Bulk stable isotope data are complemented by LMC shell data from Pellenard et al. (2011). A colour code is applied for the data per well except for stable isotope data where intensity of blue (O) and red (C) are used for differentiation. Note that a few data were obtained in the underlying "Marnes à exogyres" marls. See the text for the explanations of trends.

Figure 5: Photomicrographs of mud-supported facies (well name and sample depth are indicated on each photo header); (A) Wackestone with abundant moulds of shells (undetermined) showing a limited calcite cementation; the faint blue stain of the matrix indicates a significant microporosity ("Calcaires de Dommartin supérieurs"). (B) Wackestone with abundant small sized moulds (probably green algae; arrow) and larger vugs probably corresponding to solution-enlarged moulds; the faint blue stain of the matrix indicates a significant microporosity ("Calcaires tachetés"). (C) Bioclastic wackestone with echinoderm debris often pyritised (E), oyster shells (O), fragments of agglutinated foraminifers (arrows), and cemented moulds of bivalve shell debris; the blue stain indicates a limited patchy microporosity, possibly linked to the presence of a partially calcite-cemented microfracture on the left side of the photo ("Pierre châline"). (D) Tight wackestone with oyster shells; blue-dyed epoxy impregnation is limited to the vicinity of some microfractures, here open.

Figure 6: Photomicrographs of the “Oolithe de Bure” Member (well name and sample depth are indicated on each photo header); (A) Porous bioclastic and peloidal grainstone with (1) an early calcite cement present as isopachous rims around grains and dirty syntaxial overgrowths around echinoderms, and (2) a later clear calcite cement as isolated equant crystals and as overgrowths after the first stage. Note the abundant moulds devoid of calcite rim. (B) Closely packed bioclastic and peloidal grainstone with a fitted fabric, and with cements only present around echinoderm debris (E). (C-D) PPL and CL views of calcite cements; early cements show a dull cloudy luminescence (1) and the later clear cements a show a nice sector zoning (2).

Figure 7: SEM photos of micrites (well name and sample depth are indicated on each photo header); (A) Granular euhedral to clustered texture (Type II sensu Kaczmarek et al., 2015) with crystal sizes below 4-5µm (“Calcaires de Dommartin supérieurs”). Porous granular subhedral texture (Type I sensu Kaczmarek et al., 2015) with crystal sizes below 4-5µm, and showing rounded micro-moulds (arrows; “Calcaires tachetés”). (C) Tight clustered to fitted texture (Type II to Type III sensu Kaczmarek et al., 2015) with crystal sizes below around or above 5µm (“Calcaires sublithographiques”). (D) Tight clustered texture (Type II to Type III sensu Kaczmarek et al., 2015) with crystal sizes below around or above 5µm (“Calcaires de Dommartin inférieurs”).

Figure 8: SEM photos and distributions of crystal size for 2 micrite samples at the base and top of EST-1203 well. Note the slightly different textures and the shoulder to slightly coarser crystals in the lower sample.

Figure 9: Illustration of the macrofacies characteristics of the “Calcaires du Barrois” Formation. In the upper part the cores are discontinuous and damaged due to a 2-phase karst alteration re-using networks of burrows (A), whereas they are more continuous in the lower part unaffected by karst alterations (B). In the upper part stylolithes are rare, thin and low amplitude (A’), whereas they are abundant and thick in the lower part (B’). Microfractures are present all through the formation but mostly present in the lower half, appearing open or partially calcite-cemented (C, D).

Figure 10: $\delta^{18}O$-$\delta^{13}C$ cross-plot of all bulk and shell data. Outliers are explained by specific particularities (see details in the text). Red arrows illustrate the stratigraphic evolutions observed along the curves with increasing upward $\delta^{18}O$ of shells also associated with a slight decrease of bulk-$\delta^{13}C$ (see the text for detailed explanation).

Figure 11: Box plots of $\delta^{18}O$ (left) and $\delta^{13}C$ (right) values of micrites (bulk) and shells in the 3 wells. Note the net increase of shell $\delta^{18}O$ values from EST-1218 to EST1201 (stratigraphic increase), and the

slight increase of bulk values; shell $\delta^{13}C$ values remain stable whereas bulk values are decreasing from EST-1218 to EST-1201.

Figure 12: Porosity-permeability cross-plot of the "Calcaires du Barrois" limestones. The data are in line with the classical values of microporous oil and gas reservoirs, close to the Lucia (2007) class 3, or aligned with the "universal microporosity line" (Ehrenberg, 2019) and the Lonoy (2016) microporus mudstone transform.

Figure 13: Box plots of porosity (left) and permeability (right) per well. Note the increase of porosity from EST-1218 to EST-1201. Permeability only significantly increases between EST-1203 and EST-1201.

Figure 14: Distribution of Young's Modulus values through the "Calcaires du Barrois" along with the GR trace (opposite scales), and of semi-quantitative estimates of fracture and stylolite intensity. A clear boundary appears around 75m above which the evolutions of Young's Modulus and GR signal dissociates (see the text for explanations).

Figure 15: $\delta^{18}O$ and $\delta^{13}C$ in the 3 reference wells with their initial depths. Circles are bulk values and crosses are shell values, black arrows are bulk trends and grey arrows are shell trends. Note the separation of bulk and shell values towards the top in each well.

Figure 16: (A) Direct comparison between the $\delta^{18}O$ and $\delta^{13}C$ of bulk and shell values through the interval of overlap between EST-1201 and EST-1203. (B) Box plots of $\delta^{13}C$ values of micrites (bulk) and shells in the 2 wells. Bulk $\delta^{18}O$ values are similar in both wells, but bulk $\delta^{13}C$ are systematically lower in EST-1203 than in EST-1201 in this common stratigraphic interval.

Figure 17: Evolution of total vs 48h porosity as points (left) and curves (centre), and evolution of the S48 ratio (right), through the "Calcaire du Barrois" Formation. Note the upward decrease of the S48, overall through the whole stratigraphic interval, but also individually along each well.

Figure 18: (A) Direct comparison between the porosity and permeability through the interval of overlap between EST-1201 and EST-1203. (B) Box plots of porosity and permeability in the 2 wells. Both porosity and permeability are lower in EST-1203 than in EST-1201 in this common stratigraphic interval.

Figure 19: Young's Modulus-GR (discretised) cross-plot with bubble size as a function of porosity (values are indicated). Note the negative correlation between Young's Modulus and GR in the lower half of the formation.

Figure 20: Young's Modulus-porosity cross-plot with bubble size as a function of GR value (values are indicated). Note the weak negative correlation between Young's Modulus and porosity in the lower half of the formation. In this lower half, samples with porosity exceeding 10% form a distinct cloud.

Figure 21: Schematic representation of the "Calcaires du Barrois" Formation at the Jurassic-Cretaceous Unconformity (JCU). Freshwater invaded the upper half of the formation leading to an early meteoric diagenesis, whereas the lower half did not undergo the same flows and evolved during burial and chemical compaction. The darkness of blue colour is proportional to the clay content.

Figure 22: Schematic representation of the "Calcaires du Barrois" Formation nowadays, illustrating the petrophysical and mechanical properties acquired during diagenesis. Deformation linked to the Cenozoic orogens was mostly accommodated by and interval between the intra-formational boundary (top of "Calcaires de Dommartin inférieurs") and the "Oolithe de Bure" Member.

Figure 23: Hydrogeological model of the upstream zone of the karstic aquifer of the "Calcaires du Barrois" Formation (modified from Andra, 2022). The model proposes the definition of 2 sub-aquifers, one lower captive and one upper free, bounded by the "Pierre châline" Member. It is proposed here that the lower part of the upper free aquifer, between the "Pierre châline" and the top of the "Calcaires de Dommartin inférieurs" behaves like the captive lower sub-aquifer.

Table Captions

Table 1: Stable isotope data obtained on bulk rocks (micrites) and LMC shell values (from Pellenard et al., 2011).

Table 2: Results of the triaxial tests performed on 6 reference sample for the quality-check of the Schmidt hammer-based method.

Bulk samples					LMC shells				
Wells	Z (m)	Z cumulative (m)	$\delta^{18}O‰_{(PDB)}$	$\delta^{13}C‰_{(PDB)}$	Wells	Z (m)	Z cumulative (m)	$\delta^{18}O‰_{(PDB)}$	$\delta^{13}C‰_{(PDB)}$
	21.8	21.8	-1.5279798	1.79547822		20.85	20.85	-0.03	2.5
	23.9	23.9	-1.7869843	1.76902269		20.85	20.85	-0.49	1.81
	25.9	25.9	-1.6119037	1.39393098		20.85	20.85	-0.02	2.4
	27.9	27.9	-1.2589875	1.55199519		34.2	34.2	0.91	3.25
	29.9	29.9	-2.2009534	0.12597289		34.2	34.2	-0.27	2.18
	31.9	31.9	-2.823238	-0.904538		43.12	43.12	-0.02	2.98
	33.9	33.9	1.34881353	2.22329241		43.12	43.12	0.45	3.54
	35.9	35.9	-0.2502241	2.16615453		43.12	43.12	-0.13	3.13
	37.9	37.9	-1.1673892	1.98871465		43.12	43.12	-0.29	2.66
	39.9	39.9	-3.4237462	1.23781247	1201	44.05	44.05	-2.2	2.24
EST1201	41.9	41.9	-0.2814564	1.81090282		44.05	44.05	1.18	3.4
	43.9	43.9	-1.8051456	1.78614439		44.05	44.05	-2.16	1.61
	45.9	45.9	-2.1309256	1.59710963		44.05	44.05	0.64	3.26
	47.9	47.9	-1.7554697	1.90330092		45.84	45.84	0.17	2.9
	49.9	49.9	-1.8038238	1.97651038		45.84	45.84	0.21	3.06
	51.9	51.9	-1.9826866	2.10709965		53.43	53.43	0.81	3.16
	53.9	53.9	-1.2492231	2.24579216		57.29	57.29	-0.61	2.54
	55.9	55.9	-1.7299179	2.02791836		57.29	57.29	-0.94	2.17
	57.9	57.9	-1.568298	2.0486852		57.29	57.29	-0.31	2.59
	59.9	59.9	-1.6342754	2.17165902		4.89	47.39	-0.96	3.08
	3.7	46.2	-1.7693626	1.48157157		4.89	47.39	-0.1	3.28
	5.65	48.15	-1.3579218	1.69185005		4.89	47.39	0.41	3.92
	7.65	50.15	-1.8644774	1.62429105		12.1	54.6	-0.24	2.87
	9.65	52.15	-1.7630372	1.60395512	1203	12.1	54.6	-0.55	2.41
EST1203	11.65	54.15	-2.1637311	1.27394009		12.1	54.6	-2.04	3.21
	13.65	56.15	-1.6935997	1.75606177		13.8	56.3	-1.09	2.36
	15.7	58.2	-1.8041762	1.59635867		13.8	56.3	-2.17	2.43
	17.55	60.05	-2.3381557	1.71900663		35.5	78	-2	2.32

	19.65	62.15	-2.1055833	1.89439272		37.8	80.3	-1.94	2.38
	21.65	64.15	-2.0577113	2.1208133		6.44	98.44	-2.9	3.44
	23.65	66.15	-1.9822181	2.09662336		6.44	98.44	-1.44	4.08
	25.65	68.15	-1.4264672	2.1465869		6.44	98.44	-2.89	2.72
	27.65	70.15	-2.4392653	1.76799069		8.56	100.56	-2.16	2.08
	29.65	72.15	-2.155919	2.20679192		8.56	100.56	-3.07	2.5
	31.55	74.05	-1.817862	2.35381449		8.56	100.56	-2.33	2.83
	33.65	76.15	-1.874466	2.23975897		12.18	104.18	-0.13	3.37
	35.65	78.15	-2.2070089	1.90843526		12.18	104.18	-2.05	3.17
	37.65	80.15	-2.1165655	2.23993722		12.18	104.18	-0.06	3.11
	39.65	82.15	-1.6765157	2.25800814		14.06	106.06	-0.38	2.63
	41.65	84.15	-2.1058087	2.18343209		14.06	106.06	-2.47	2.59
	43.65	86.15	-3.0606641	0.94863488		17.06	109.06	-2.07	3.34
	45.65	88.15	-1.7683904	2.28671003		17.06	109.06	-1.05	2.61
	47.65	90.15	-2.0038918	2.22302033		17.06	109.06	-2.8	2.07
	49.65	92.15	-1.5196397	2.48173505	1218	19.46	111.46	0.51	3.09
	4.75	96.75	-2.2186968	1.94054357		19.46	111.46	-0.46	3.24
	6.75	98.75	-2.0030557	2.40565023		22.16	114.16	-1.63	3.31
	8.75	100.75	-2.3924293	2.42182862		22.16	114.16	0.1	3.02
	10.75	102.75	-1.6190232	2.449973		26.19	118.19	-2.12	2.96
	12.75	104.75	-2.3386997	2.17641382		26.19	118.19	-2.19	2.21
	14.75	106.75	-2.2780905	2.06639747		38.78	130.78	-2.1	2.86
	16.75	108.75	-1.5709756	2.62037824		38.78	130.78	-2.05	3.26
EST1218	18.75	110.75	-1.4919026	2.72950091		38.78	130.78	-2.43	3.37
	20.75	112.75	-1.3830099	2.73608055		41.2	133.2	-0.9	2.27
	22.75	114.75	-1.0984691	2.85658429		41.2	133.2	-1.17	2.64
	24.75	116.75	-2.6566811	2.69691825		44.96	136.96	-1.23	2.7
	26.75	118.75	-2.1552846	2.78245016		44.96	136.96	-0.23	2.87
	28.75	120.75	-2.329918	2.7361803		44.96	136.96	-1.66	2.82
	30.75	122.75	-1.6531889	2.77824935		49.6	141.6	-1.52	2.49
	32.75	124.75	-1.4490661	2.94038179		49.6	141.6	-1.5	1.98

34.75	126.75	-1.7091215	2.82098037	56.14	148.14	-1.35	2.87
36.75	128.75	-1.8421051	2.71077108	56.14	148.14	-2.5	2.6
38.75	130.75	-1.3493764	2.71629807	56.14	148.14	-0.46	3.32
40.75	132.75	-1.3149369	2.52059407	57.01	149.01	-0.2	3.3
42.75	134.75	-2.07645	2.36799018	57.01	149.01	-0.26	3.2
44.75	136.75	-1.8487306	2.2944717	57.01	149.01	-0.82	2.62
46.75	138.75	-1.915737	2.08361902				
48.75	140.75	-2.9673314	2.22754983				
50.75	142.75	-3.1019456	2.28064887				
52.75	144.75	-3.0910146	1.76812583				
54.75	146.75	-3.868049	2.21503505				

Table 1

Sample depth (top, in m)	Member	Texture	Deviatoric stress at failure (MPa)	Confining pressure (MPa)	Pore pressure (MPa)	Cohesivity (Mpa)	Internal friction angle (°)	Young's Modulus (GPa)
38.99	Oolithe de Bure	Grainstone	31.67	17.47	10	0.2	7.38	5.184
38.7	Oolithe de Bure	Grainstone	30.95	20	10			2.972
38.45	Oolithe de Bure	Grainstone	24.215	15	10			2.425
36.39	C. Dommartin inférieurs	Wackestone	297	30	10	22	37.2	49.25
37.49	C. Dommartin inférieurs	Wackestone	162.13	20	10			20.25
37.55	C. Dommartin inférieurs	Wackestone	244	40	10			39.8

Table 2

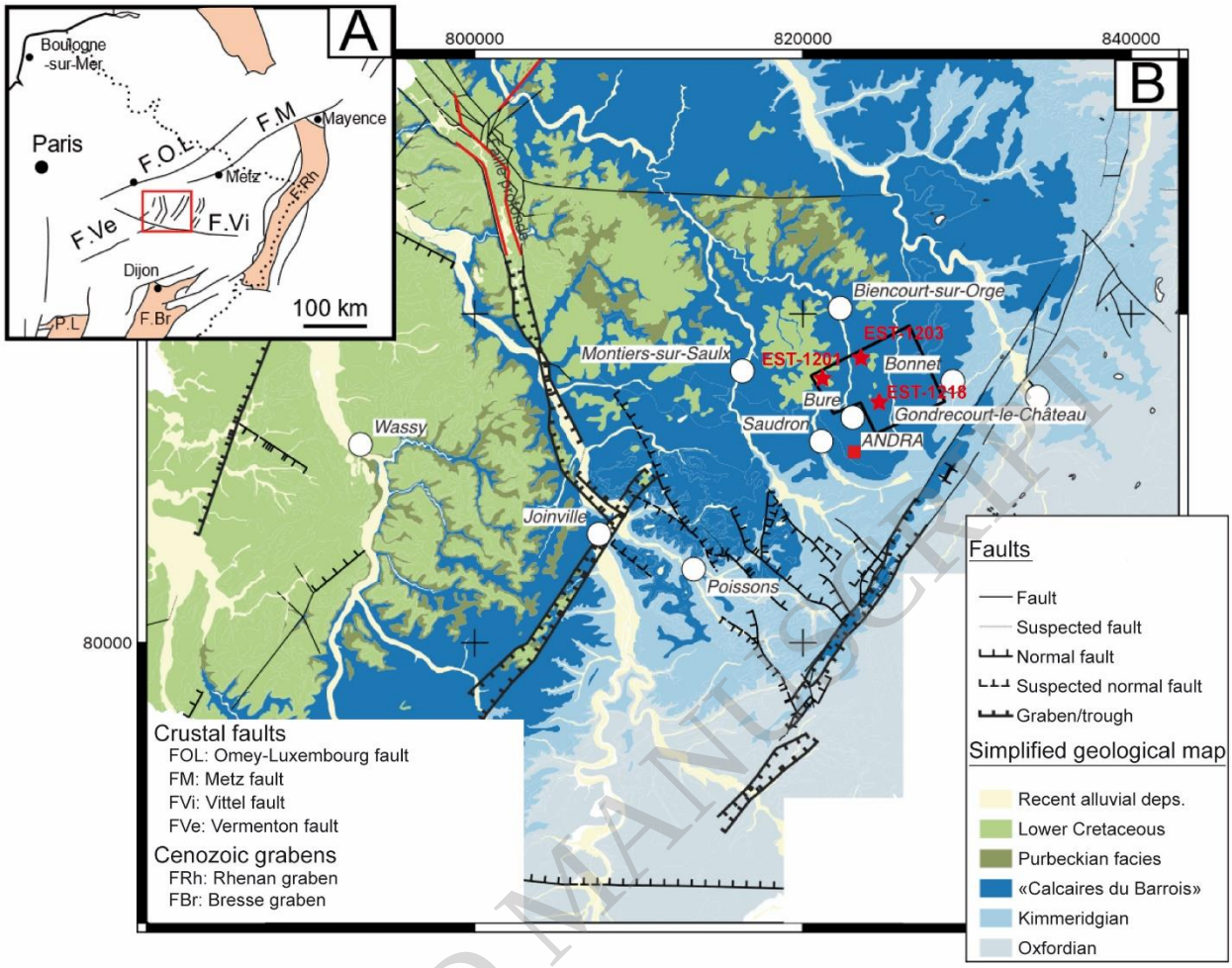

Figure 1

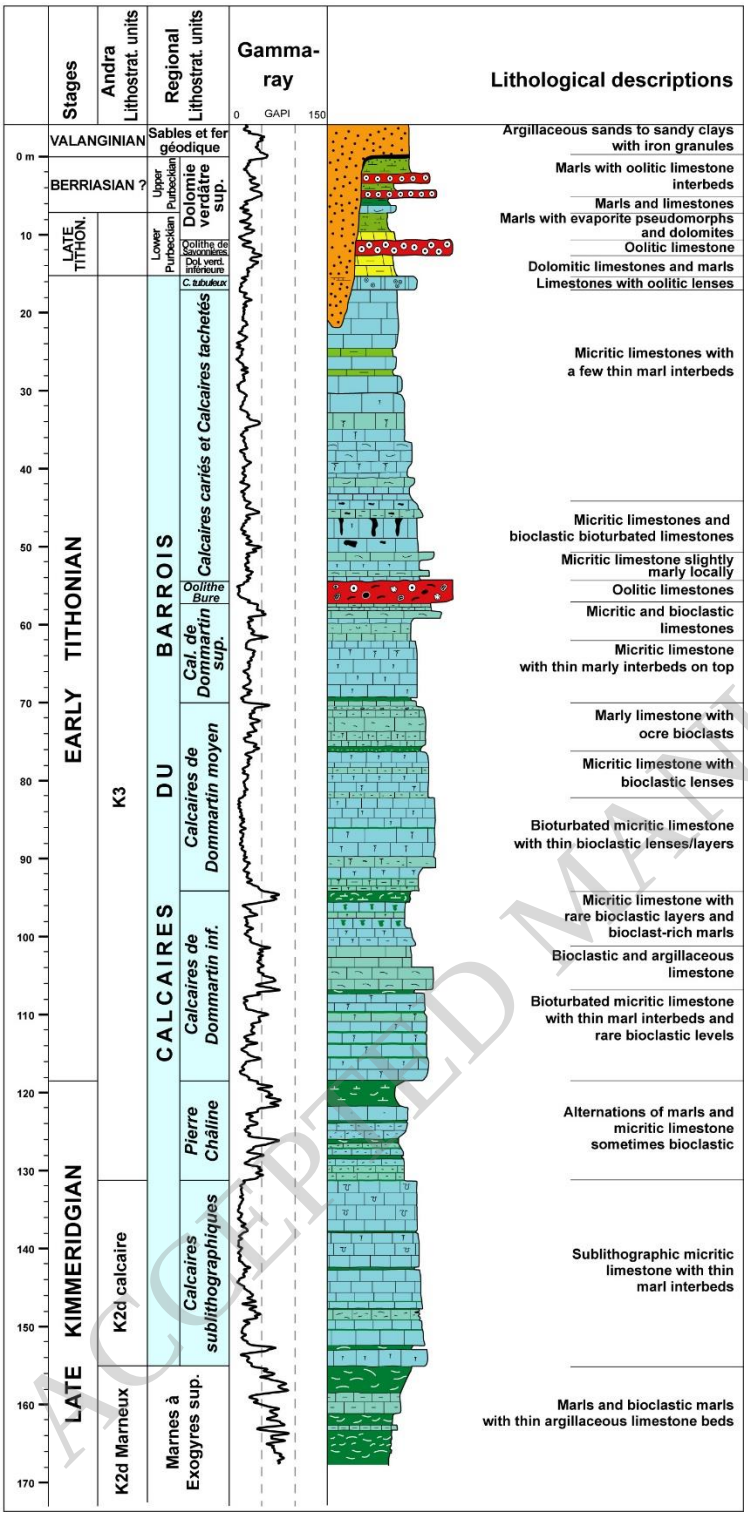

Figure 2

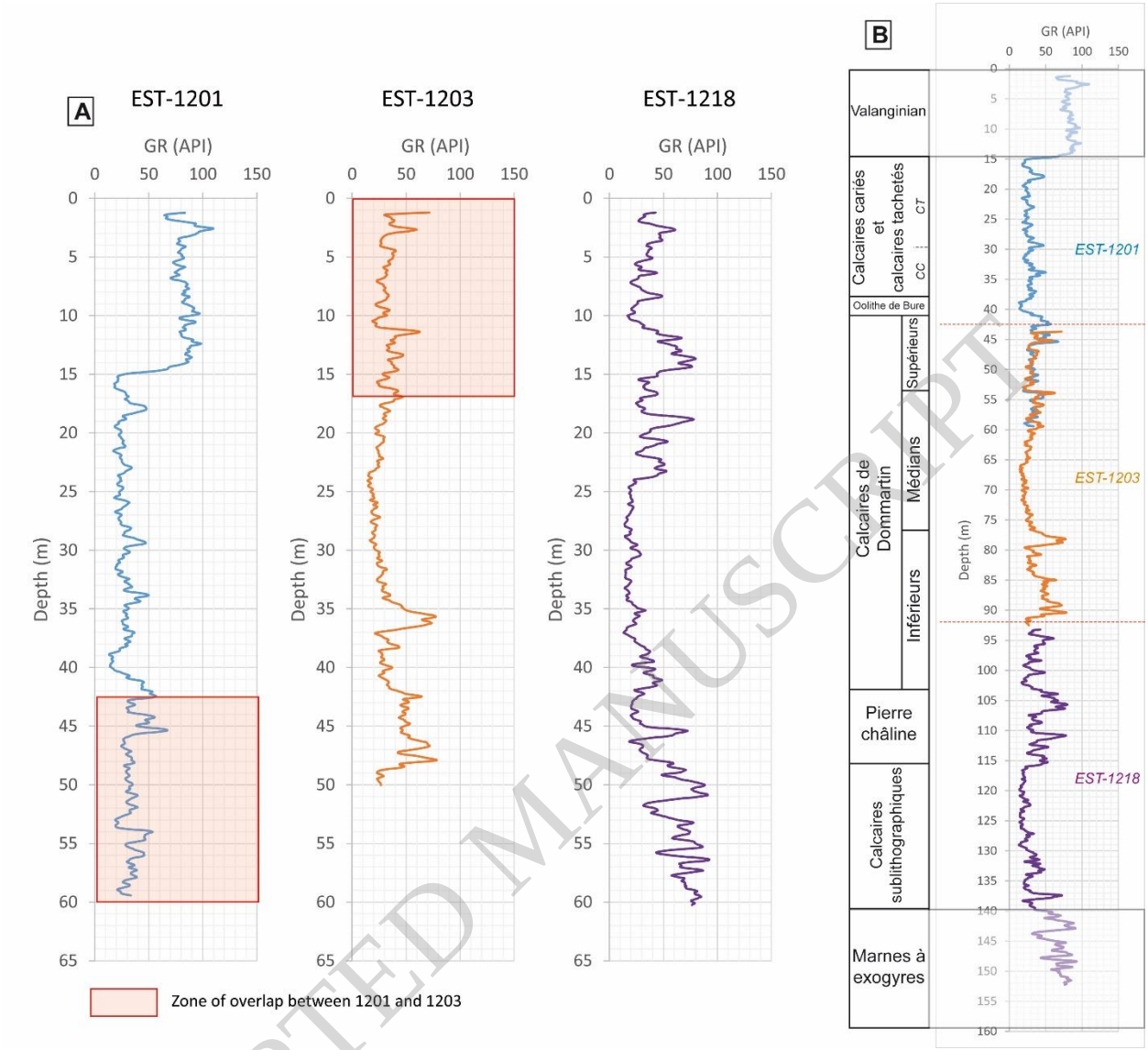

Figure 3

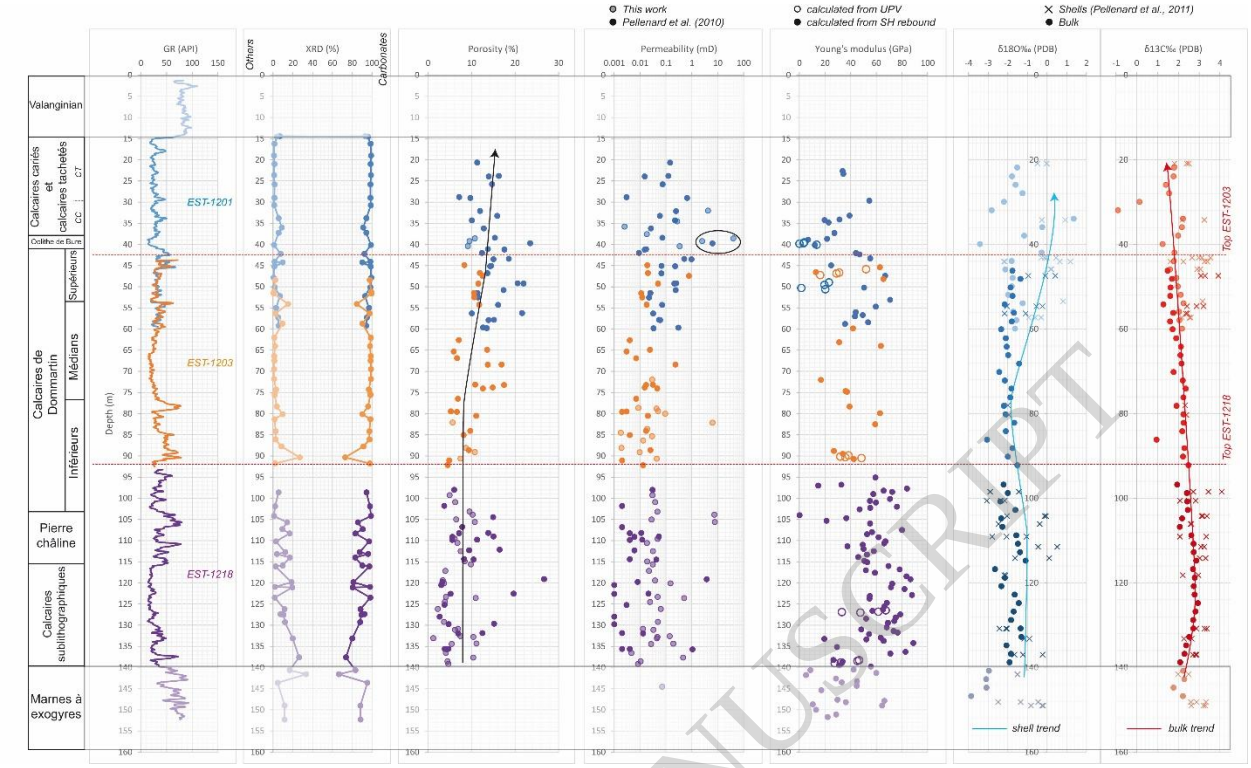

Figure 4

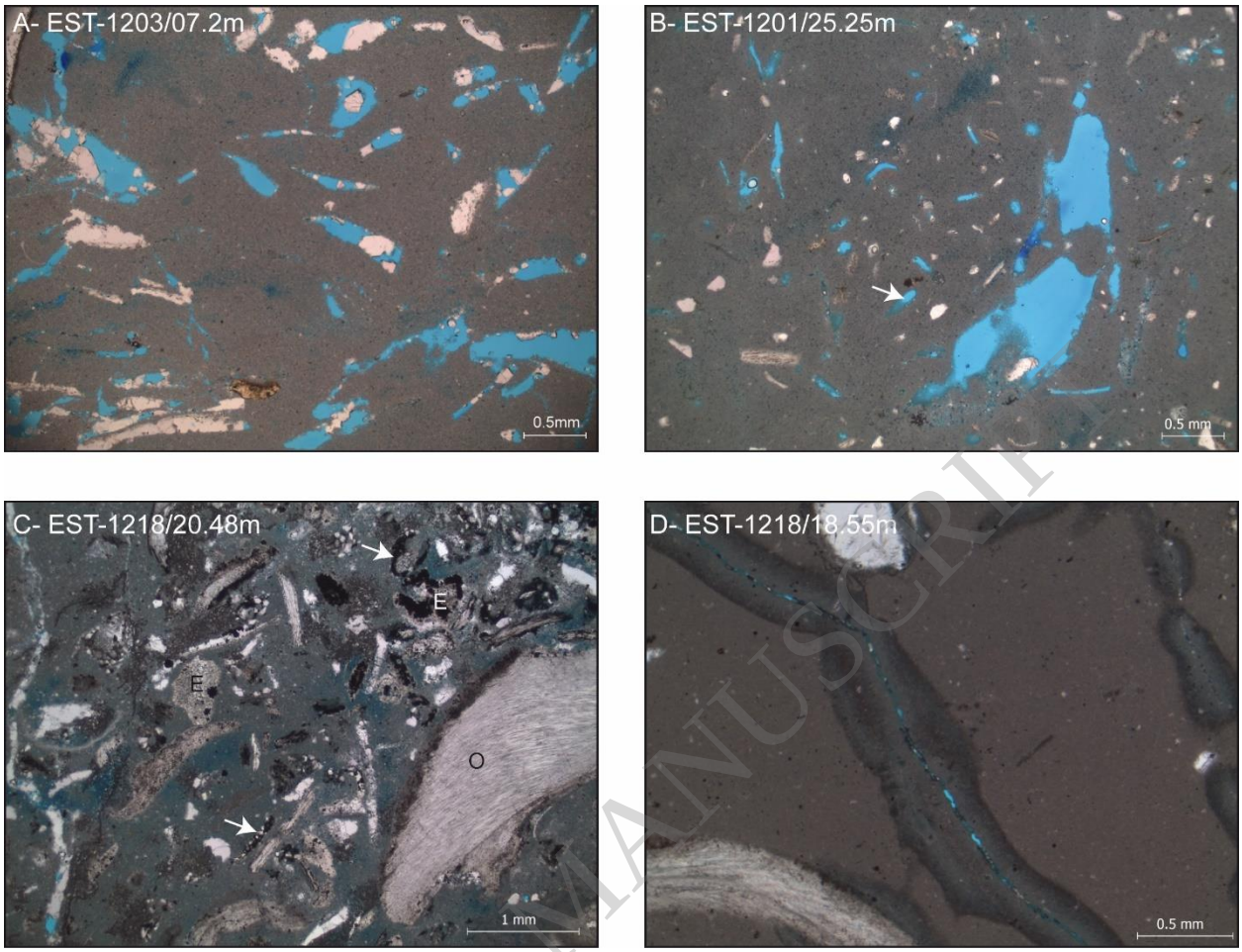

Figure 5

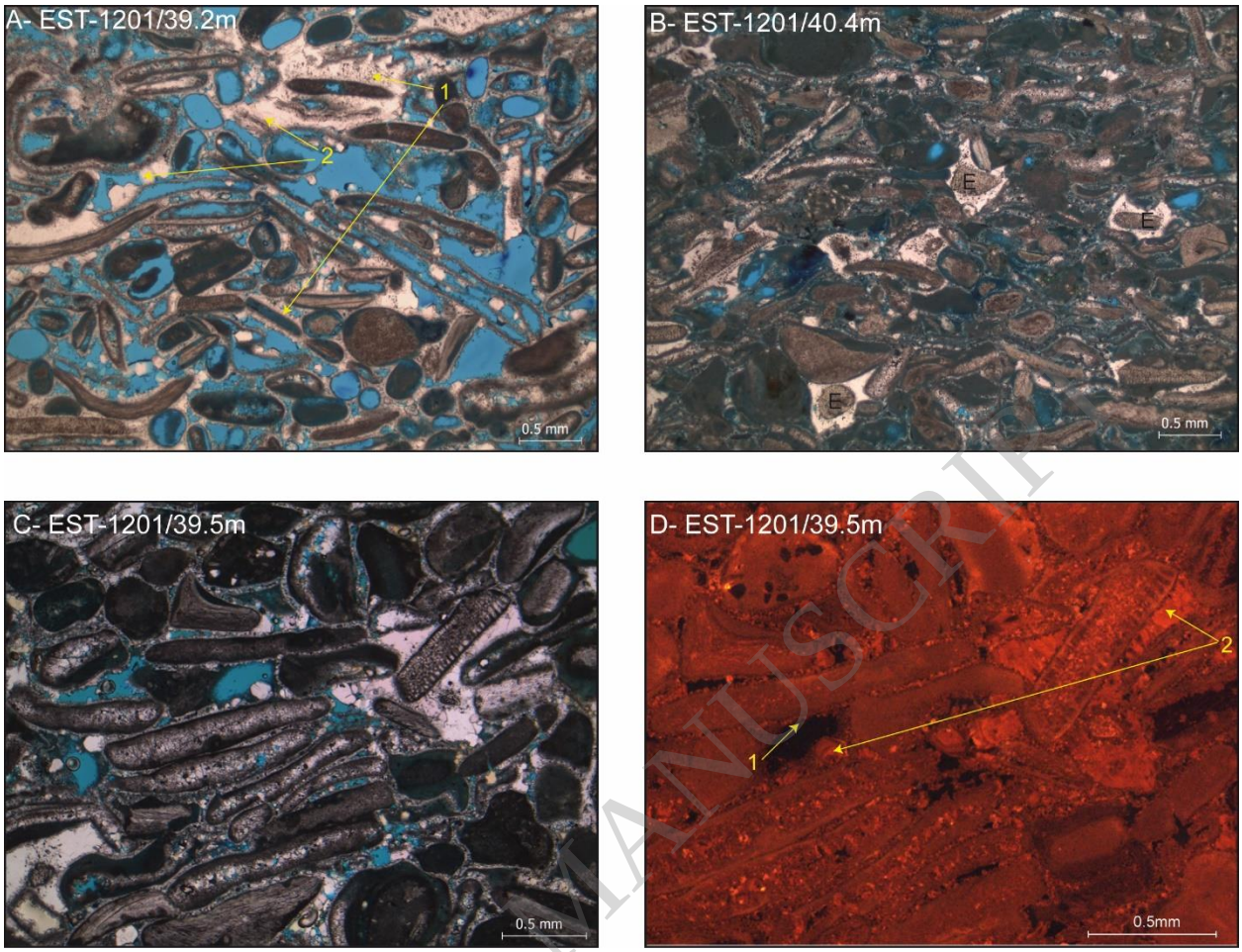

Figure 6

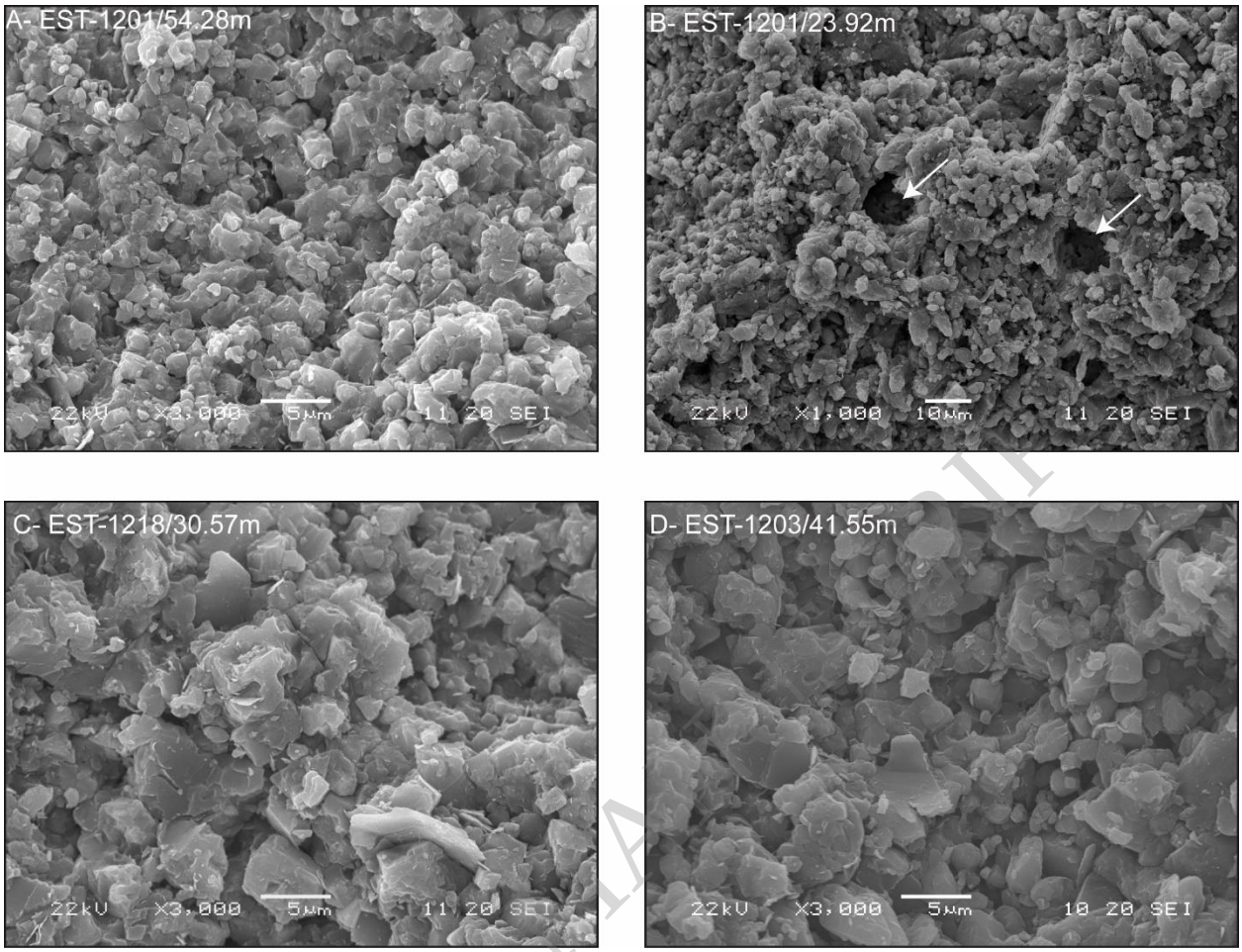

Figure 7

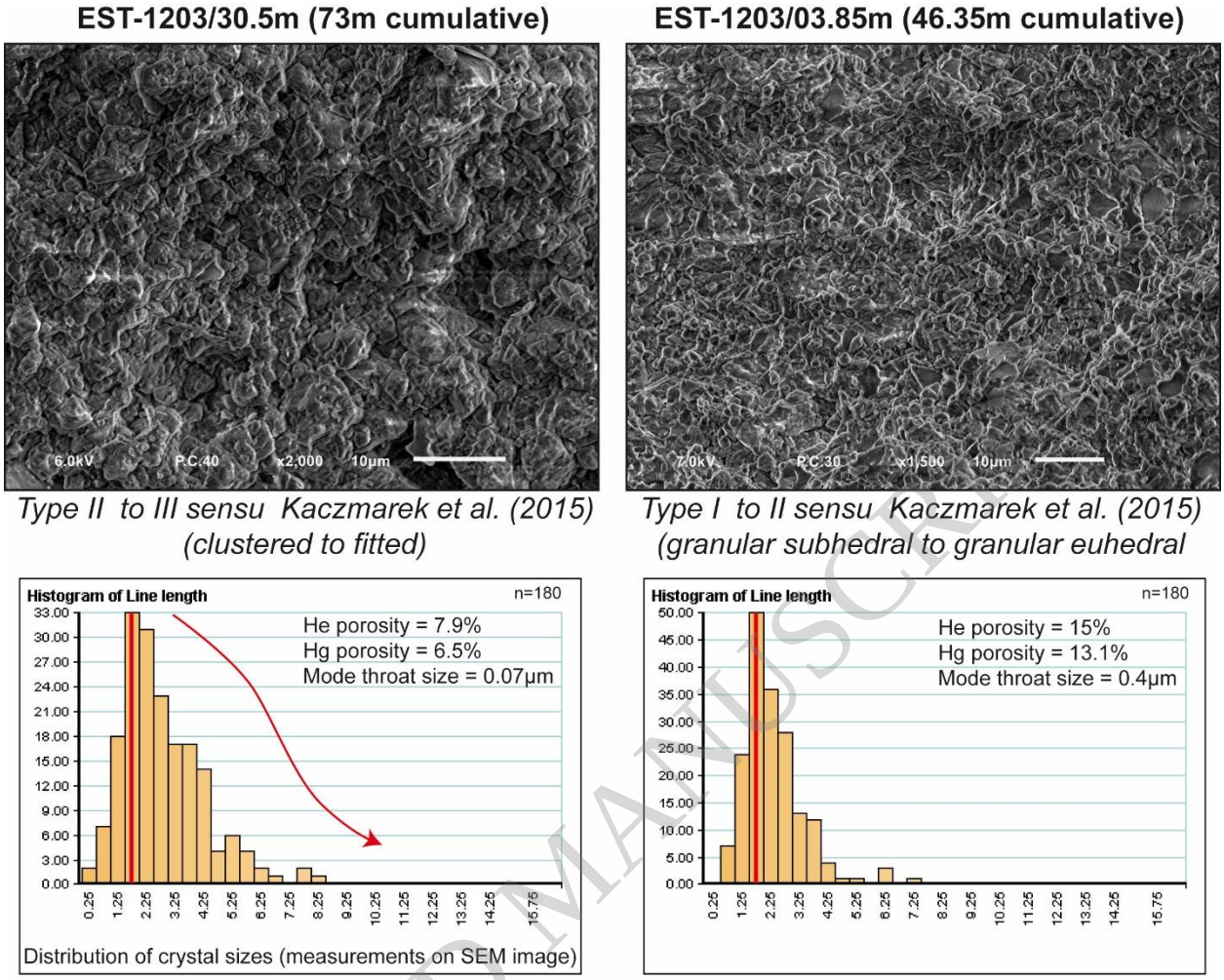

Figure 8

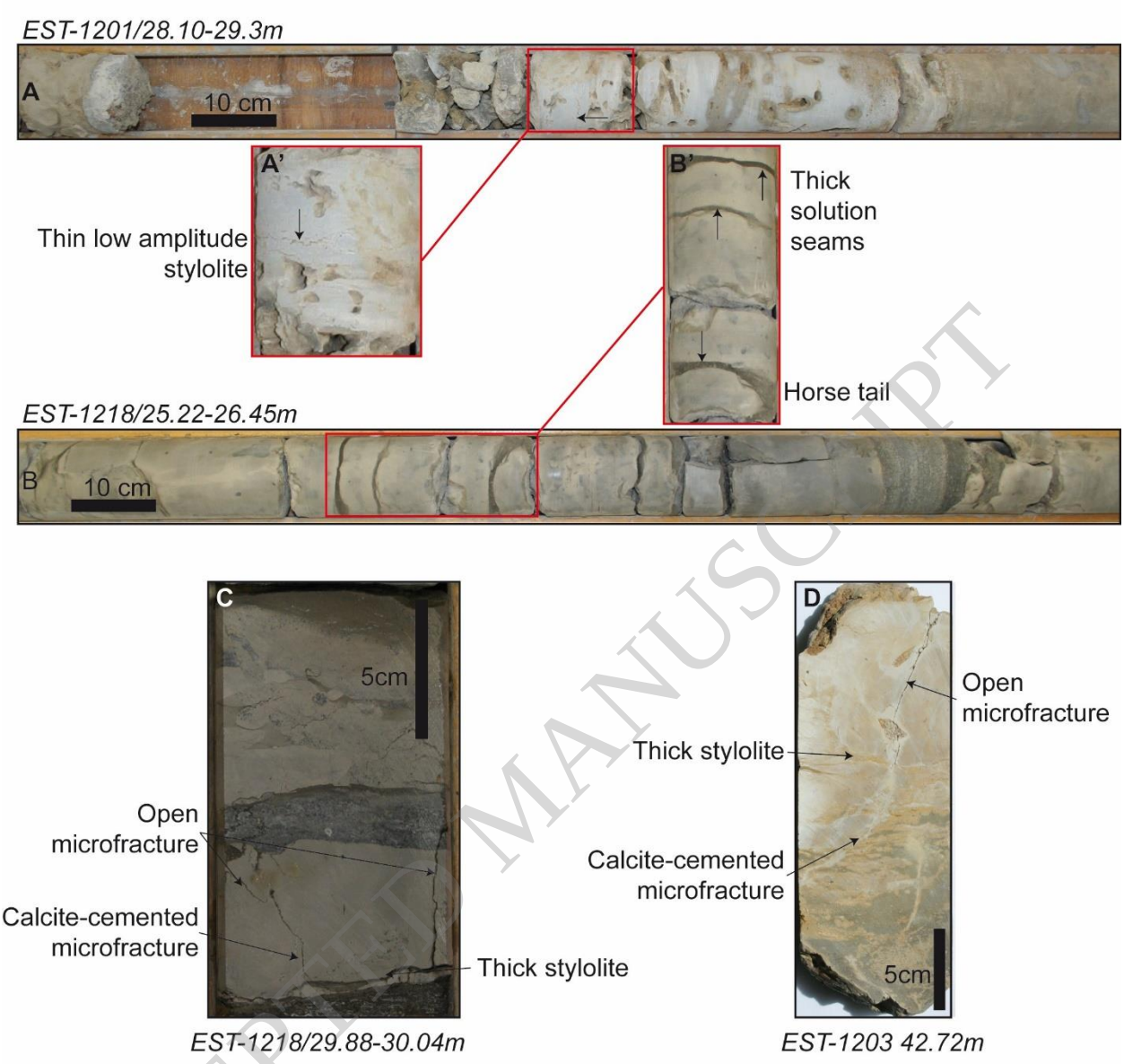

Figure 9

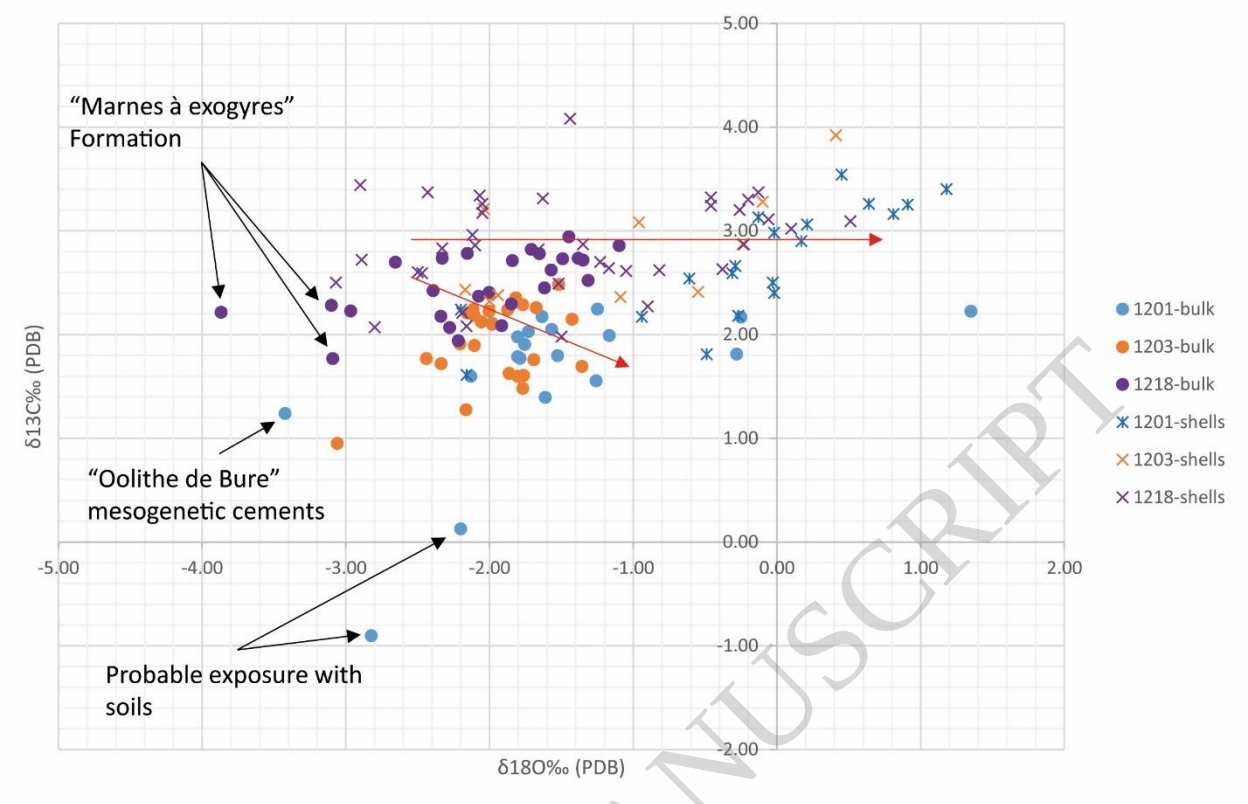

Figure 10

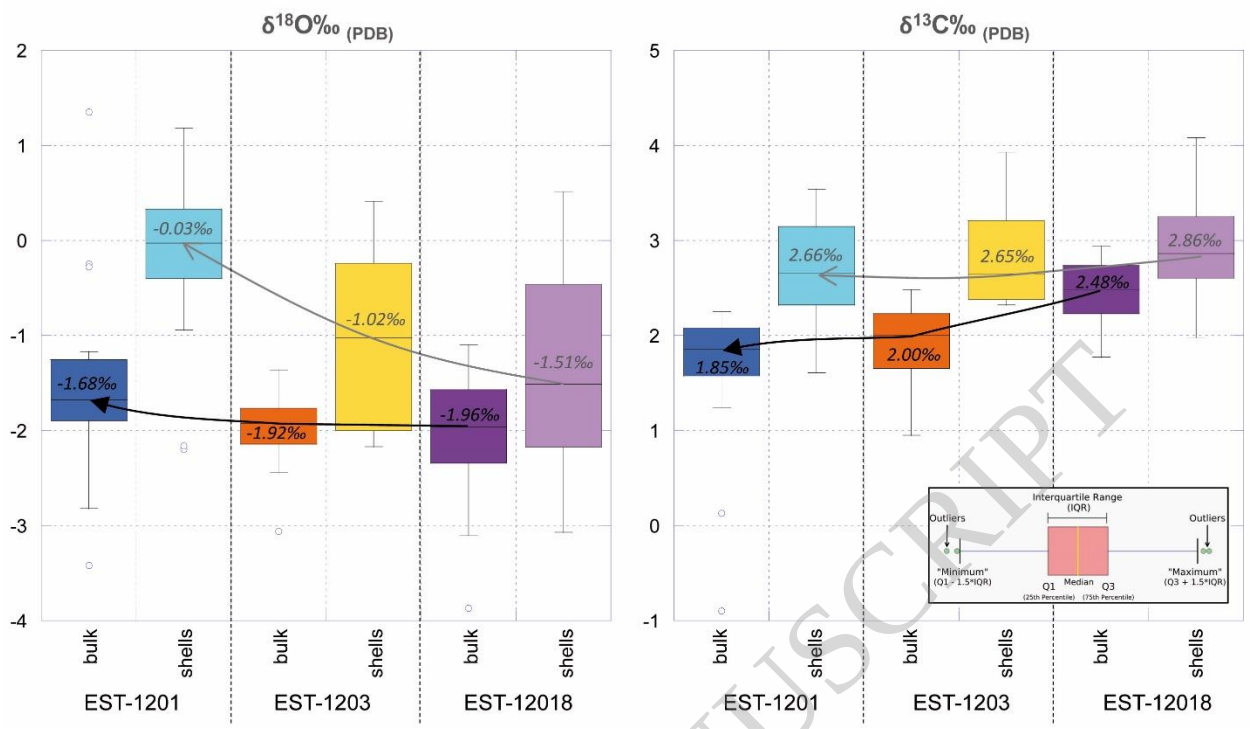

Figure 11

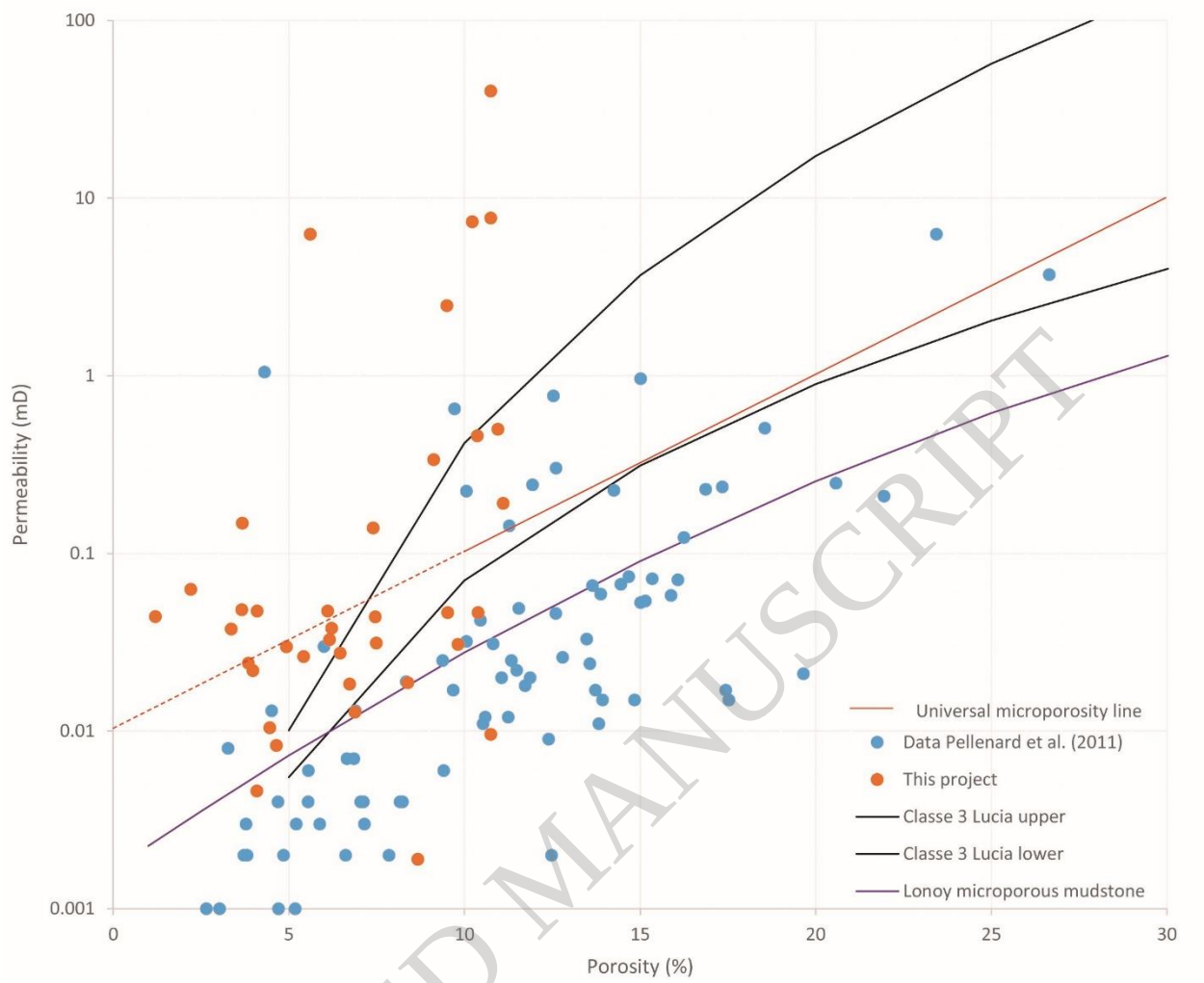

Figure 12

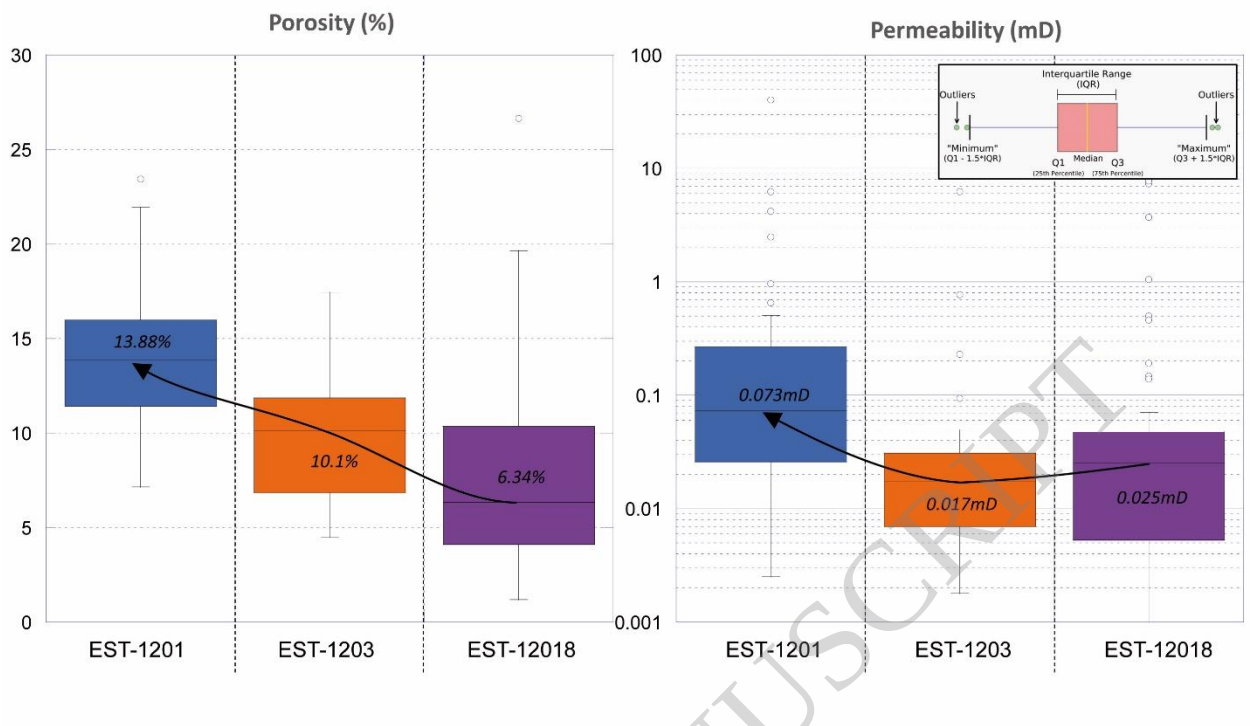

Figure 13

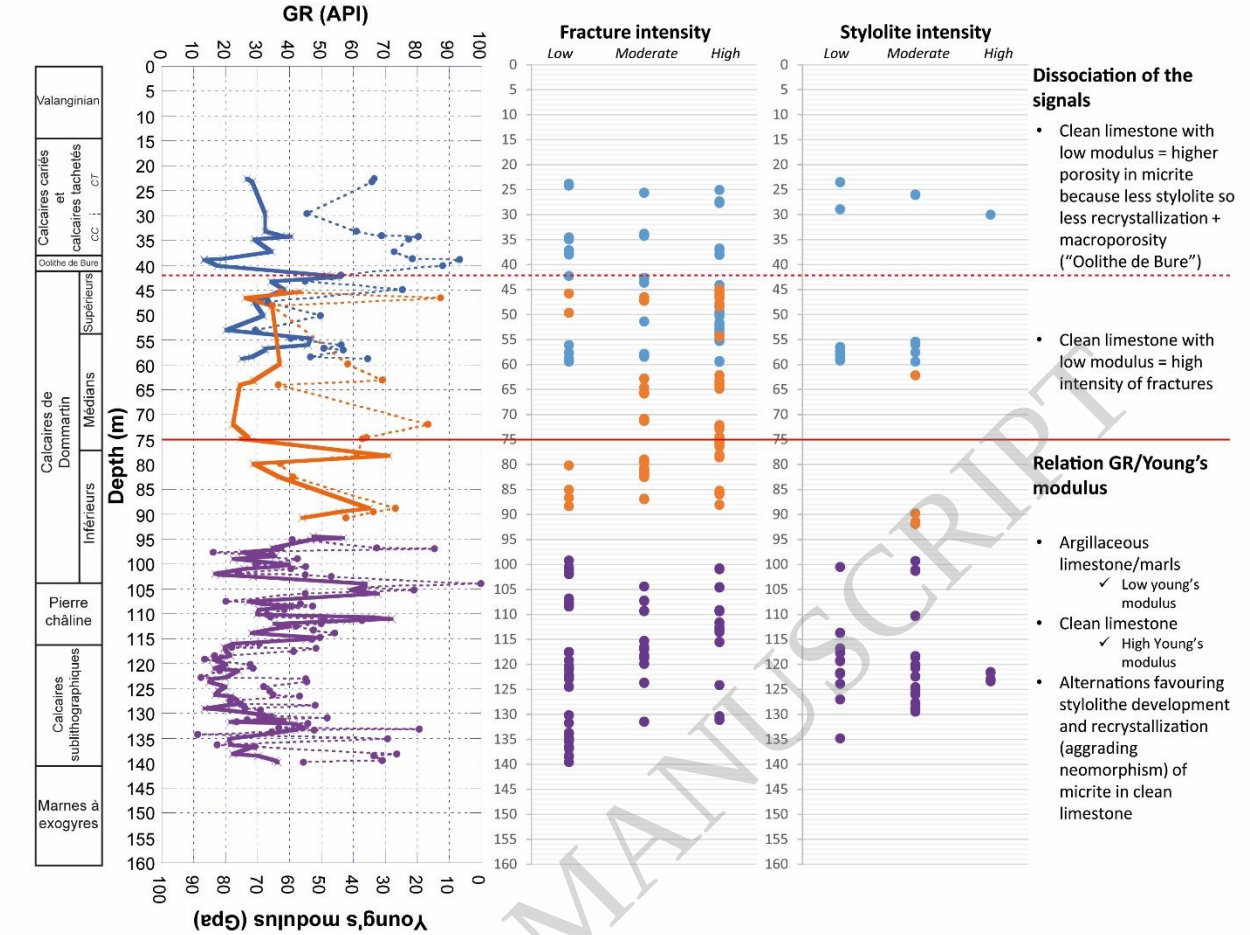

Figure 14

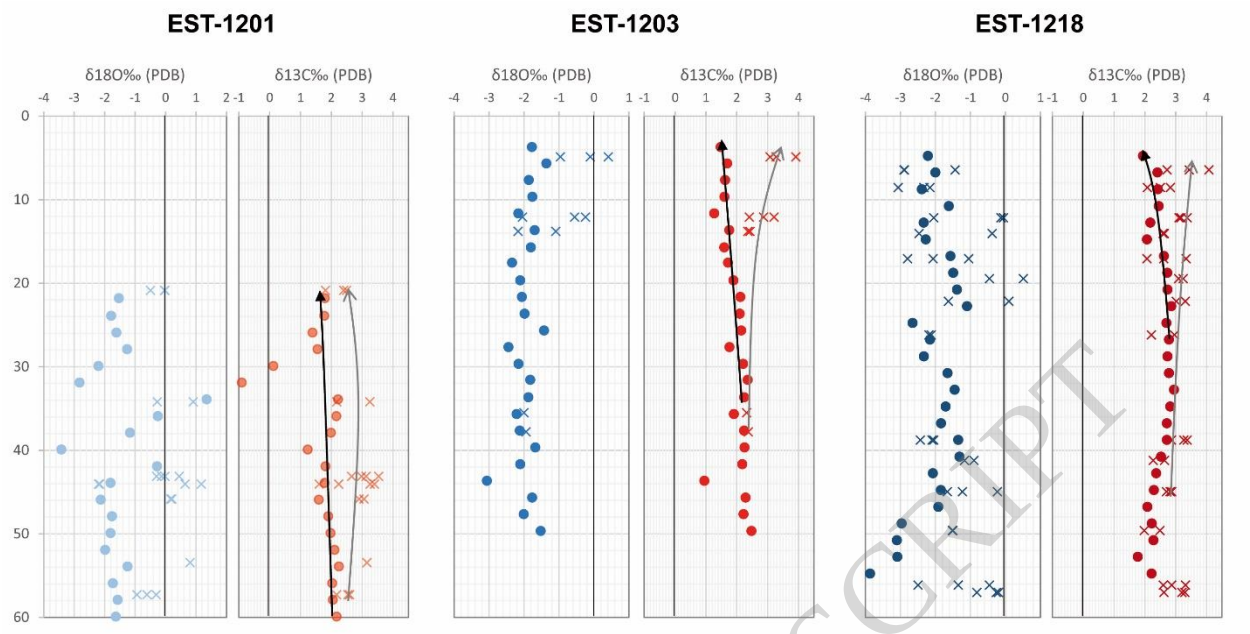

Figure 15

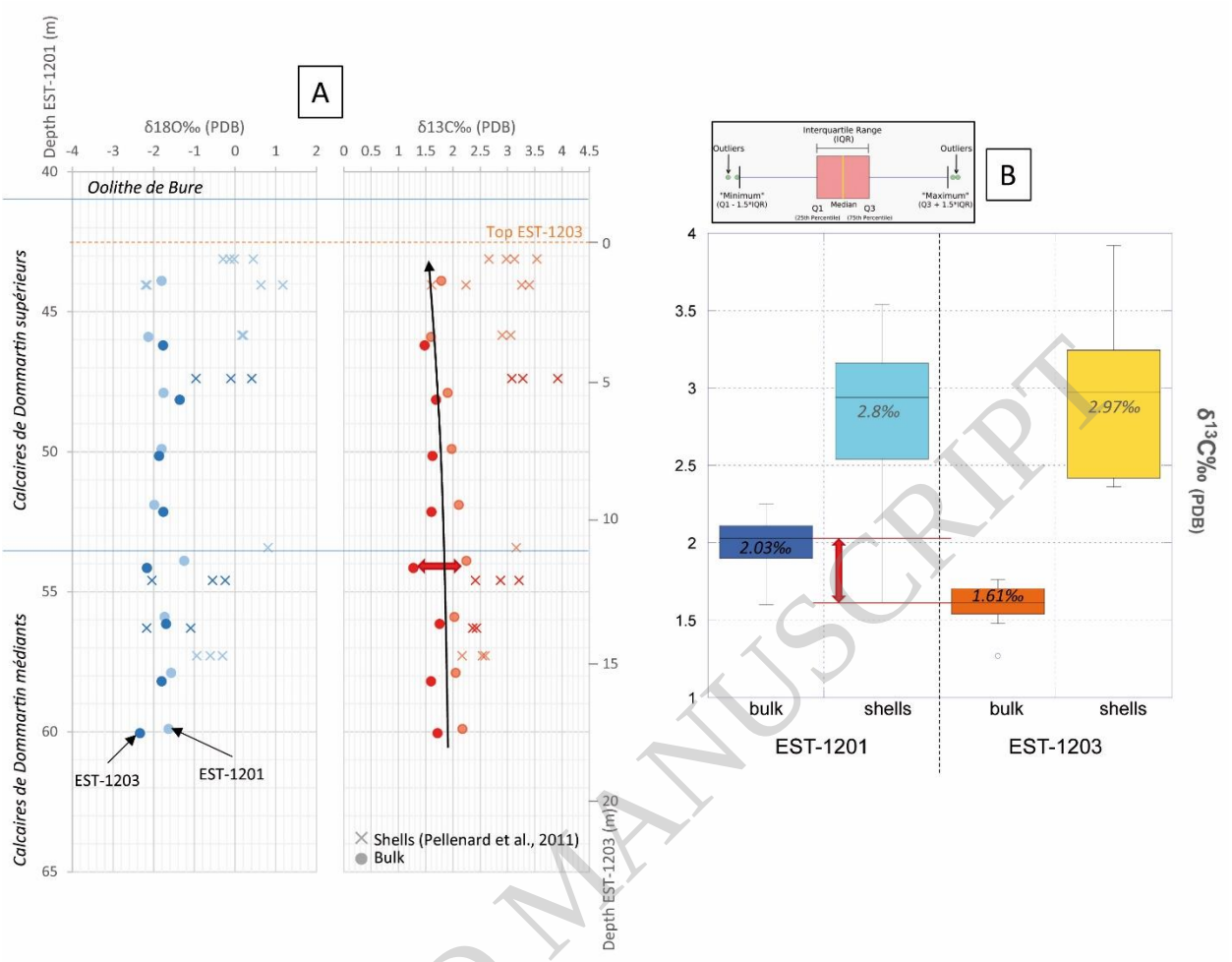

Figure 16

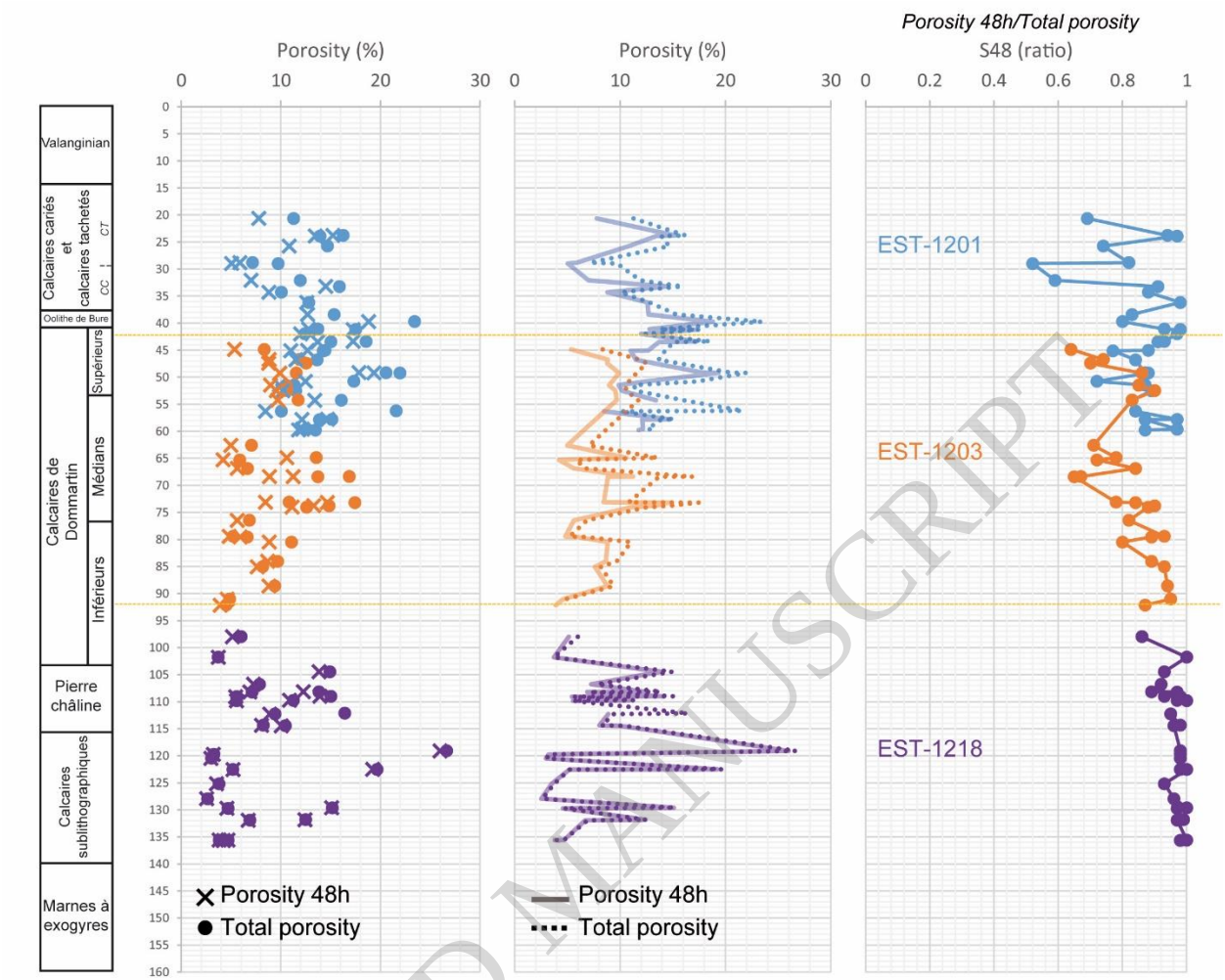

Figure 17

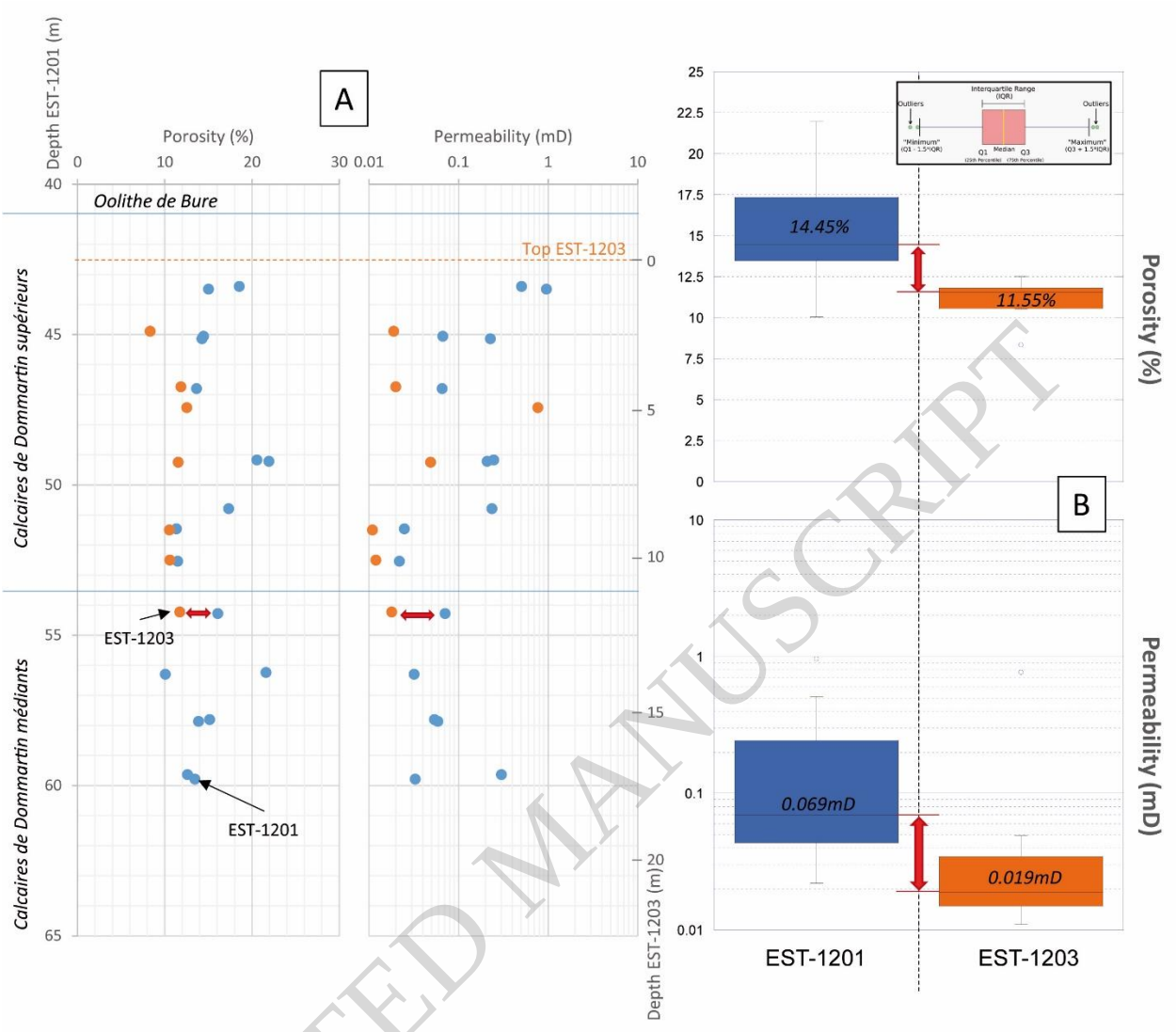

Figure 18

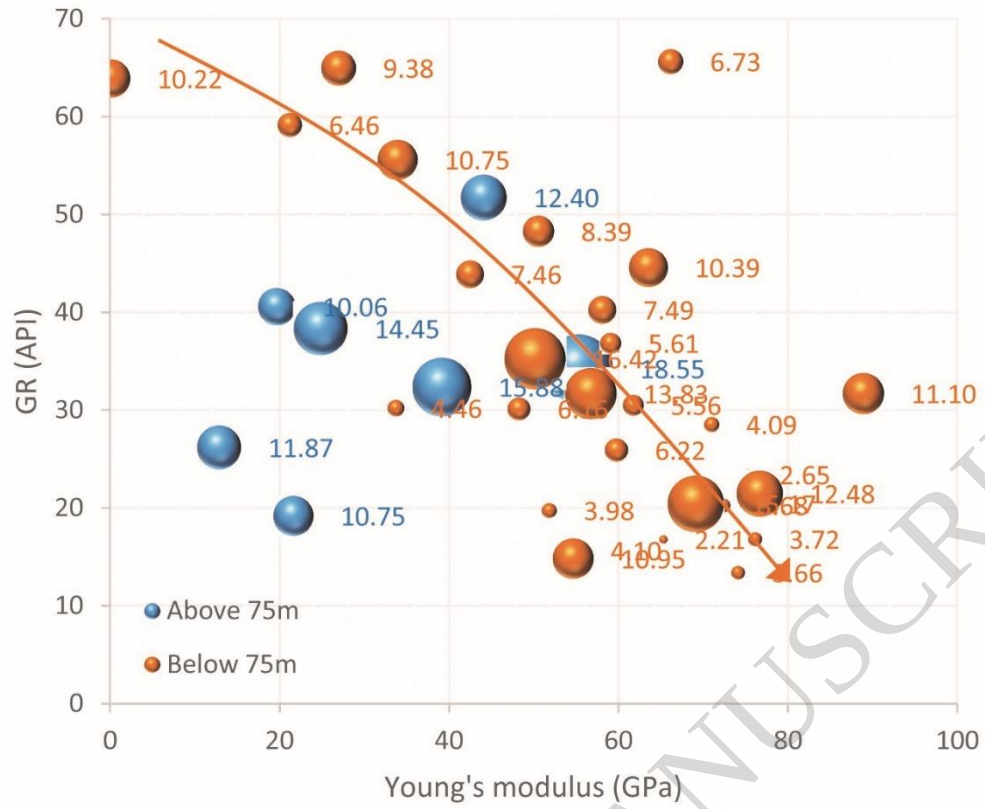

Figure 19

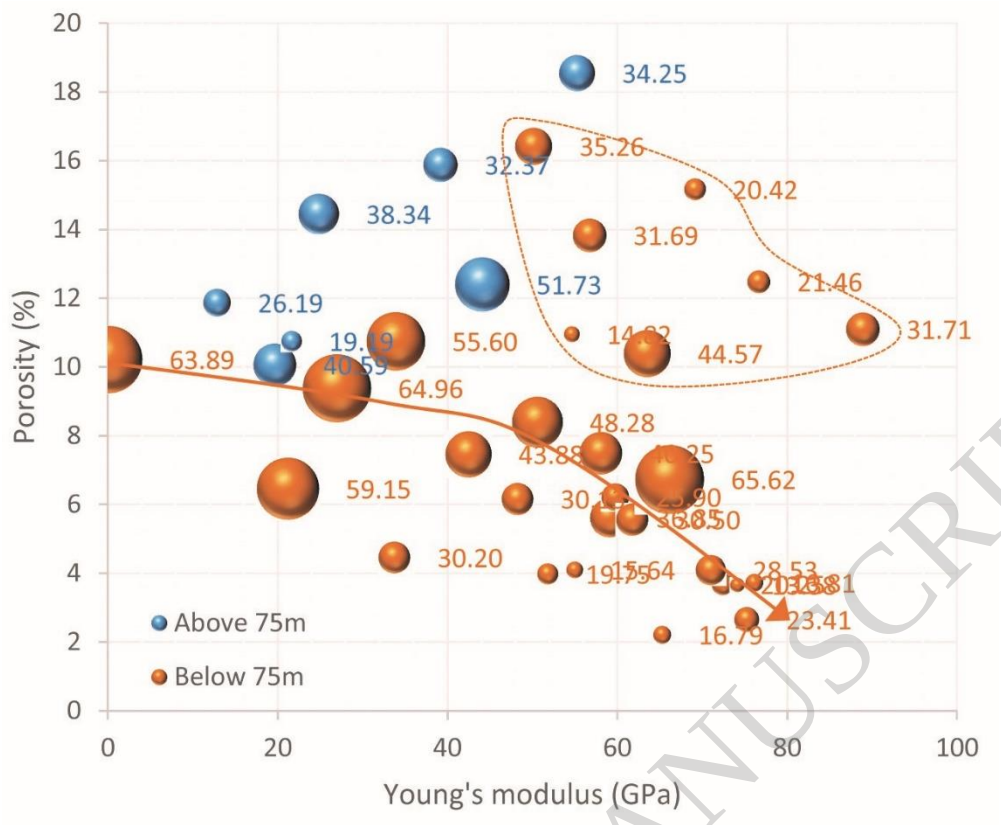

Figure 20

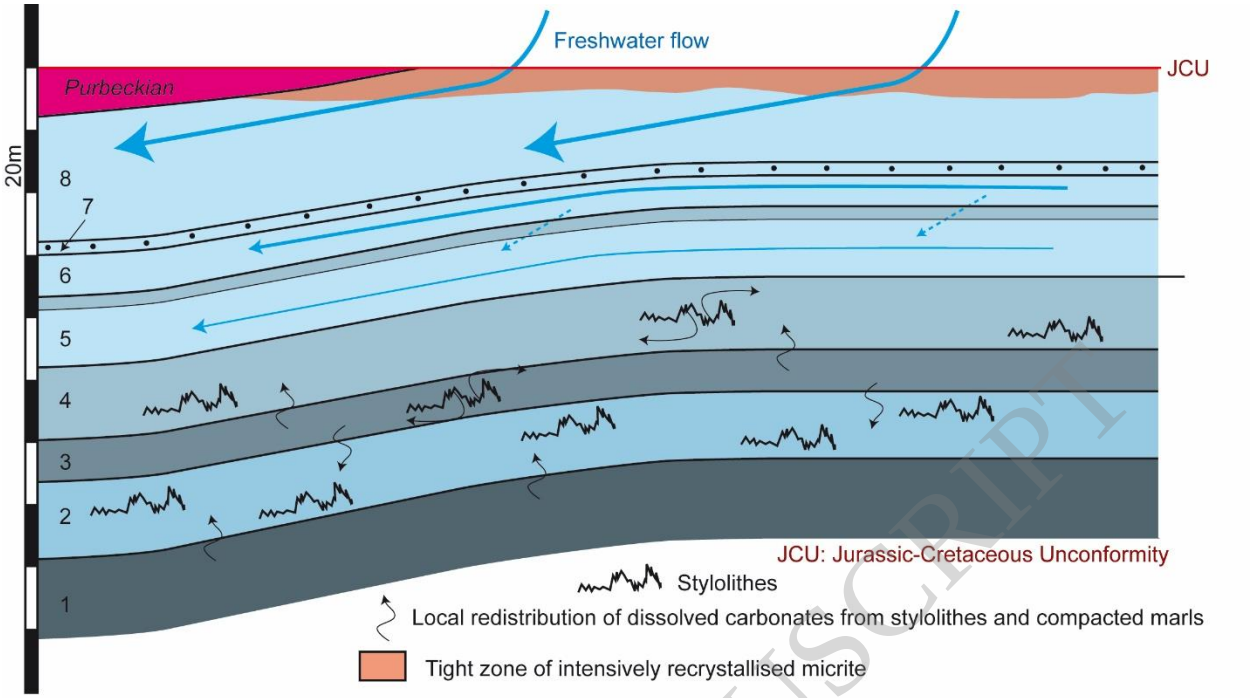

1: *Marnes à exogyres; 2: Calcaires sublithographiques; 3: Pierre châline; 4: Calcaires de Dommartin inférieurs; 5: Médians; 6: Supérieurs; 7: Oolithe de Bure; 8: Calcaires cariés/tachetés/tubuleux*

Figure 21

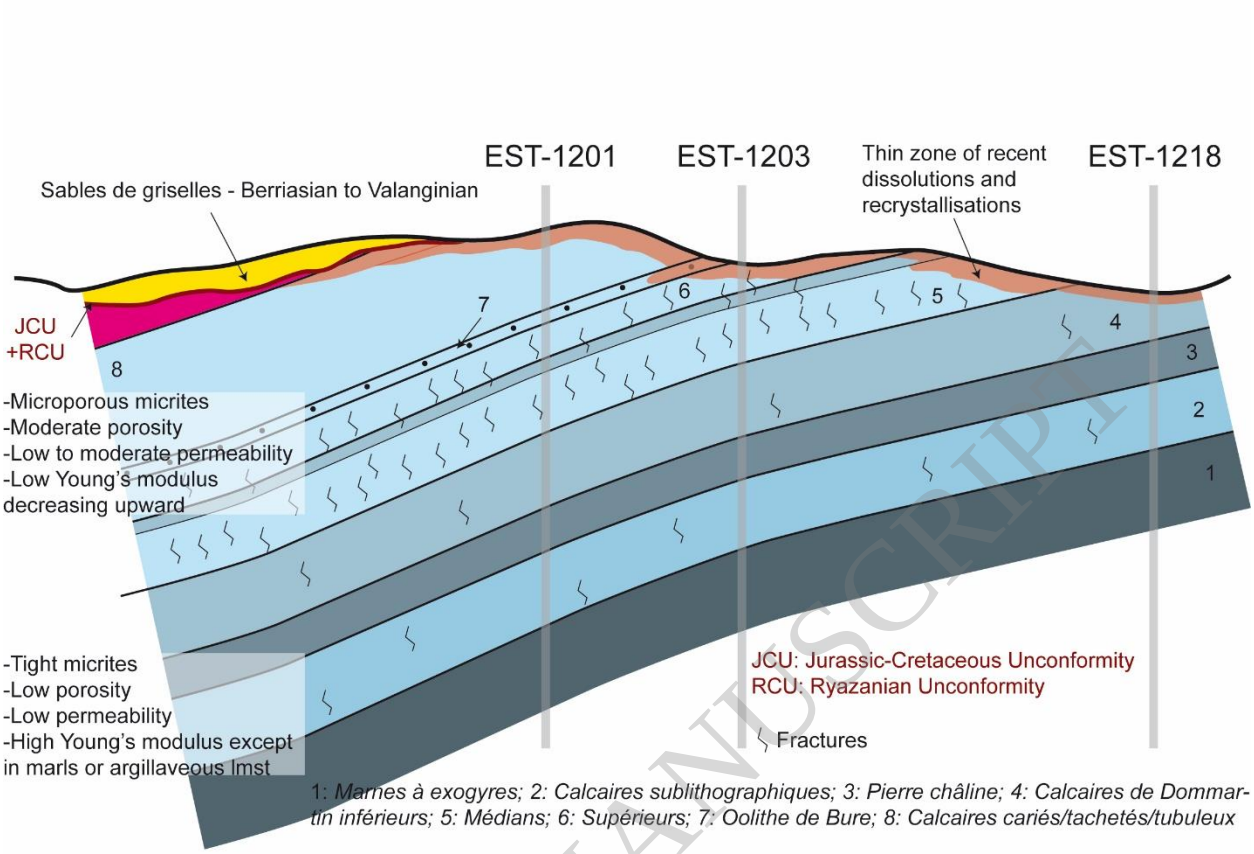

Figure 22

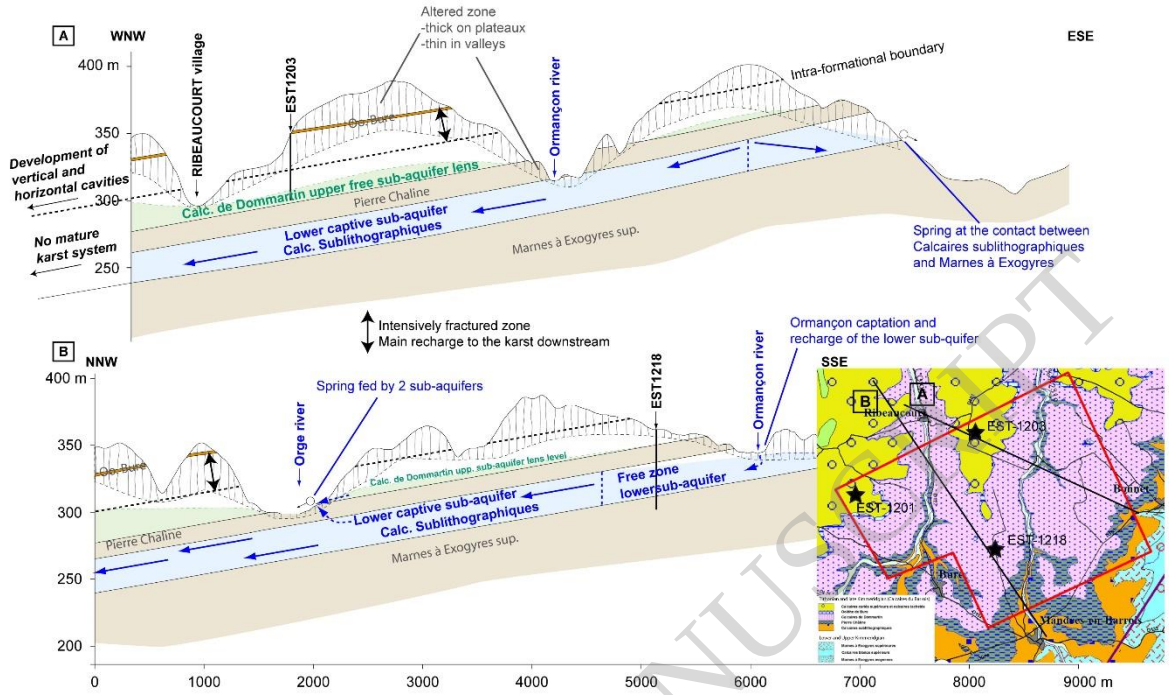

Figure 23